Università della Calabria

Dipartimento di Ingegneria Informatica,
Modellistica, Elettronica e Sistemistica

Dottorato di Ricerca in
Ingegneria dei Sistemi e Informatica
XXVI ciclo

Tesi di Dottorato

Microwave Open Resonator for Complex Surface Characterization

Hugo Oswaldo Moreno Avilés

DIMES
Novembre 2013

Settore Scientifico Disciplinare: ING-INF/02

UNIVERSITÀ DELLA CALABRIA

UNIVERSITA' DELLA CALABRIA

Dipartimento di Ingegneria Informatica, Modellistica, Elettronica e Sistemistica

Dottorato di Ricerca in

Ingegneria dei Sistemi ed Informatica

CICLO

XXVI

Microwave Open Resonator for Complex Surface Characterization

Settore Scientifico Disciplinare 09 –ING-INF/02

Direttore: Prof. Sergio Greco

Firma

Supervisori: Prof. Giuseppe Di Massa

Firma

Prof.ssa. Sandra Costanzo

Firma

Dottorando: Dott. Hugo Oswaldo Moreno Avilés

Firma

to my wife, Ximena, for all her support and love
to my angel, Francis,
to my little princess, Sofia,
to my parents, for them love.

Acknowledgements

First my thanks to God for all the mercy, the blessings, and beautiful grace during this studies period shared with my lovely family and great people.

This research has been performed in the Microwave Lab of the University of Calabria (UNICAL), in Calabria, Italy, with the Group of Electromagnetism.

I am very grateful of Professor Giuseppe Di Massa, My Tutor, who has proposed this research topic to me and has rigorously followed and contributed to my research. I would like to thank him for his constant support and great scientific discussions.

I would like to thank to Professor Sandra Costanzo, My co-Tutor, who contributed my research and taught me the right way to do it, for all her time and advices and for let me the chance to share my knowledge.

To the team of the Microwave Lab, specially to Mr. Enio Marozzo, great gentleman and professional, a extraordinary Sir, to Eng. Antonio Borgia, a colleague and a good friend for his selfless help and support, specially in the measurements periods and his charisma and love to my daughter, to all my PhD colleagues, Alireza, Ali, Antonio, Francesco and David, for all the interesting scientific discussions.

To the old DEIS (Dipartimento de Elettronica Informatica e Sistemistica) at UNICAL, all the staff, who gave me friendliness, kindness and courtesy in all this period.

I would like to acknowledge the financial support by the "Secretaria Nacional de Educacion Superior, Ciencia y Tecnologia" (SENESCYT) and the "Escuela Superior Poltecnica of Chimborazo", Ecuador. None of this research

would have been possible without their financial support.

I would like to thank to Dr. Romeo Rodriguez, Rector of the ESPOCH, Ivan Menes, Dean of the Informatics and Electronic Faculty and Paul Romero, Director of the Electronic Engineering School for all their unconditional support.

I am really grateful with my family, my wife and my daughter for all their support, patience and love, to my parents for their love, the education gave to me from my born day and the time shared with me, my brothers and sisters for the huge experiences lived together.

Sincerely

Hugo

Preface

This Ph.D. thesis contains the result of research undertaken at the "Microwave Lab" in the DIMES Department "Dipartimento di INGEGNERIA INFORMATICA, MODELISTICA, ELETTRONICA E SISTEMISTICA" of the UNICAL University of Calabria over a period of three years (2010-2013). Certainly, I would have never reached the point of finishing my Ph.D. without the help and support of others.

Starting as the first foreign Ph.D. student at the Microwave Lab, the work began under the supervision of Prof. Giuseppe Di Massa and Prof. Sandra Costanzo who gave me all the information and material of the all previous research done about microstrip reflectarray antennas, that include new synthesis algorithm and new design techniques.

Microstrip antenna design supposes to know the relative permittivity value of the dielectric substrate provided by the manufacturer, but in microwave applications a little change in the permittivity value gives some considerable variation in frequencies bands, then, it was necessary to study and find a system to measure the real value of the permittivity in terms of frequency. A period of lectures and articles arrived.

Some few weeks later, after getting used with the language, the lab and dielectric measurements techniques, an amazing article title "Open resonator powered by a rectangular waveguide", 1992, written by Bucci and Di Massa, my Supervisor, arrived in my hands, in original version. Open resonator theory, explained in Chapter 1, with parabolic approximation to the wave equation was my daily bread to understand how it works and how to make the coupling between a waveguide and the cavity and at the end to find a simple equivalent circuit that express all the system.

After some interesting discussions with my tutor, the idea of using the open resonator to measure the dielectric permittivity got shape and we de-

signed the system to do that and the theory to get the results getting a new approach to retrieve the value of the relative permittivity.

The construction of a hemispherical open resonator for K-band was the next step to validate the theory, firstable through the measurement of the resonance frequencies in the empty cavity, "so sensitivity but it works", and later, inserting some dielectric substrate and applying the proposed approach on the measurements to retrieve the value of the permittivity, explained in Chapter 2. The results obtained were acceptable.

The idea of the new Open Resonator Technique for measurement dielectric parameters, brought a lot of new application ideas out, but, our research must continue in the next step that was the reflectarray characterization. The best idea was characterize those type of antenna, but using the open resonator technique, exposed en chapter 3. We developed the new approach, we designed some reflecting surface and we characterized the reflection coefficient of variable size reflectarray patch elements using the proposed model with excellent results.

The idea of using the open resonator theory for new applications continued in our mind for long time, and because the research subject of the lab is microwave components and antennas, why not to develop a new theory for an Fabry Perot antenna?. In the last chapter of this thesis,this new subject is explained, a simple Fabry Perot cavity, feed by a rectangular waveguide, where the electromagnetic field cavity can be used to compute equivalent currents on radiating apertures, obtaining from them the radiated far field. The approach can be adopted for the analysis as well as for the synthesis of a large variety of cavity antennas.

In order to validate the approach, a Fabry-Perot antenna was fabricated for K-band and measured in the Microwave Lab at University of Calabria.

I have been involved in other collaborative works; in particular with Prof. Sandra Costanzo and Francesco Spadafora, searching for low cost radar systems for target detection and soil discontinuties detection using SDRadar systems.

Rende (Cosenza) , novembre, 2013

Hugo Oswaldo Moreno Aviles
.

Contents

List of Figures

List of Tables

Part I

Complex Surface Characterization by an open resonator Technique

1

Microwave Open Resonator

1.1 Introduction

This chapter is dedicated to treat the theory of open resonator. In the simplest case, an open resonator consists of two mirrors facing each other. The origin of Open Resonator can be dated to the beginning of the twentieth century when Charles Fabry and Alfred Perot introduced a new interferometric device which would eventually bear their name: the Fabry-Perot interferometer [1]. This novel form of interference device was based on multiple reflection of waves between two closely spaced and highly reflecting mirrors. Fabry and Perot published a large number of papers on their interferometer, including 15 joint articles between 1896 and 1902.

The subject of laser resonator by the use of a Fabry Perot interferometer has proposed in independently way in ([2]-[4]). The theory for resonators with spherical mirrors and the approximation of the modes by waves beams was proposed in [5, 6], but, the concept of electromagnetic wave beams was introduced in [7, 8] where was investigated the sequence of lens for the guided transmission of electromagnetic waves. The theories are based on a scalar formulation, which, although it is sufficient for most purposes, ignores the vector nature of the electromagnetic field.

In [9] an electromagnetic theory of the open resonator was done, where, the standing wave fields are obtained by the superposing of those fields that are due to two highly directional beams propagating in opposite directions along the axis of symmetry of the device.

The use of open resonator either in the microwave region, or at higher frequencies (optical regions) has taken place over a number of decades. The related theory and its applications have found a widespread use in several branches of optical physics and today is incorporated in many scientific in-

struments [10].

In microwave region open resonators have also been proposed as cavities for quasi-optical gyrotrons [11]and as an open cavity in a plasma beat wave accelerator experiment [12].

A vector formulation of electromagnetic Gaussian beam was introduced in [13], where the beam was constructed from a single components of the electric and the magnetci vector potentials that are roiented in the propagation direction of the beam. The use of Open Resonator as microwave Gaussian Beam Antennas [14, 15]and [16] provides a very interesting solution as they can provide very low slidelobes level. They are based on the result that the field map at the mid section of an open resonator shows a gaussian distribution that can be used to illuminate a metallic grid or a dielectric sheet.

For microwave application a reliable description of the coupling between the cavity and the feeding waveguide is necessary. Several papers deal with the coupling through a small hole or a rectangular waveguide taking into account only for the fundamental cavity and waveguide mode [17, 18, 19]

In [20] a complete analysis of the coupling between a rectangular waveguide and an open cavity has been developed taking into account for all the relevante eigenfunction in the waveguide and in the cavity.

This chapter reviews the general theory of Open Resonator and proposes to study the analysis made in [20], where, the coupling between a feeding coupling aperture given by a rectangular waveguide is treated.

Starting with a general description of the open resonator and treating the paraxial approximation of the wave equation, we derive the modal expansion of the field into the cavity taking into account for the proper coordinate system. The computational of the modal coefficients take into account for the characteristics of the mirrors, the ohmic and diffraction losses and coupling.

1.2 Open resonator description

The open cavity resonator consists of two, perfectly conducting, mirrors facing each other, as showed in Fig. **??**, and situated symmetrically about the xy plane along an axis of symmetry that coincides with the z axis.

The medium bounded by the two perfectly conducting concave mirrors (M) is free space and the distance between the two mirrors along the axis of

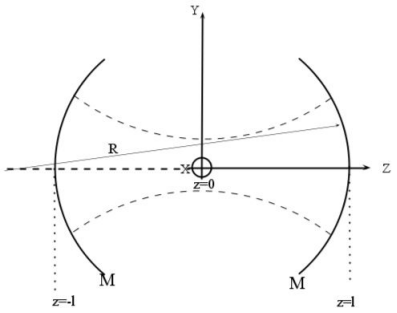

Fig. 1.1: Schematic diagram of the open-cavity resonator

symmetry is $D = 2l$. The stability of the open resonator depends of the curvature of the mirrors, non necessary equals but both of them spherical with radio R.

The phasor electric and magnetic fields in free space and bounded by the two mirrors have a harmonic time dependence $exp(-iwt)$, where w is the wave angular frequency.

1.3 Stability of Open resonator

A resonator with spherical mirrors of unequal curvature is representable as a periodic sequence of lens which can be stable or unstable. The stability condition assumes the form:

$$0 < \left(1 - \frac{2l}{R_1}\right)\left(1 - \frac{2l}{R_2}\right) < 1 \tag{1.1}$$

The above expression was previously derived in [6] from geometrical optics approach based on equivalence of the resonator and a periodic sequence of parallel lens and independently in [7] solving the integral equation for the field distribution of the resonant modes in the limit of infinite Fresnel numbers.

To show graphically which type of resonator is stable and which is unstable, it is useful to plot a stability diagram on which each type of resonator type is represented by a point. This is shown in Fig. 1.2 where parameters d/R_1 and d/R_2 are drawn as the coordinate axes; unstable systems are represented by points in the gray area and stable systems are represented by the points in the blue area.

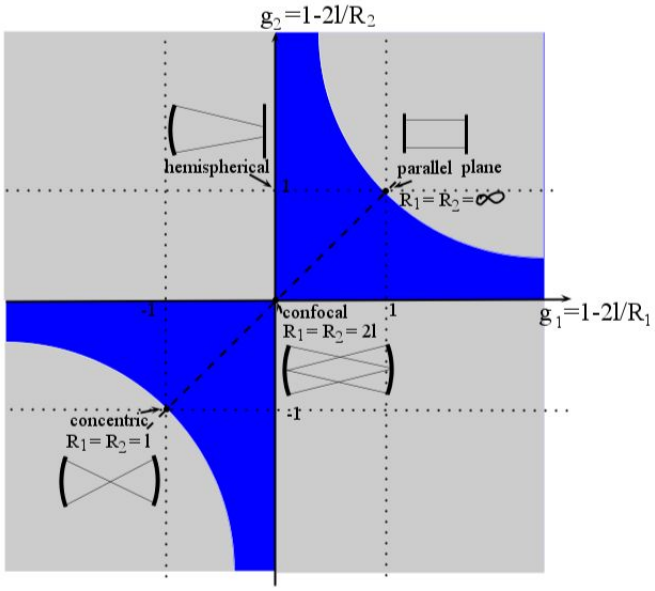

Fig. 1.2: Stability diagram of an open resonator

1.4 Wave analysis by Parabolic Approximation

The parabolic equation is an approximation of the wave equation which models energy propagating in a cone centred on the paraxial direction as show in Fig. 1.3. A parabolic equation was first introduced into the analysis of electromagnetic wave propagation in [21] and [22] in the 1940s. Since then, it has been used in diffraction theory to obtain approximative (asymptotic) solution when the wavelength is small compared to all characteristic dimensions. As open resonators usually satisfy this condition, the parabolic equation finds wide application in developing a theory of open resonators.

A field component of a coherent wave satisfies the scalar wave equation:

$$\bigtriangledown^2 \mu + k^2 \mu = 0 \tag{1.2}$$

where $k = 2\pi/\lambda$ is the propagation constant in the medium.

For a wave travelling in the z direction, assuming an e^{jwt} time dependence, the field components can be expressed as:

$$\mu = \Psi(x, y, z)\, e^{-jkz} \tag{1.3}$$

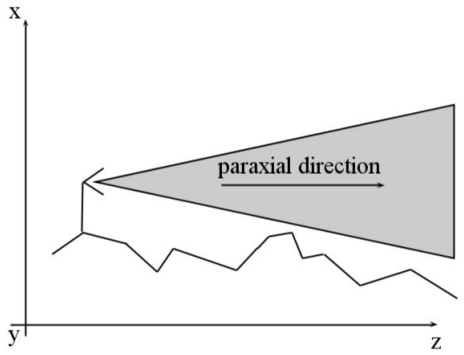

Fig. 1.3: Propagation of Energy in paraxial direction

where Ψ is a slowly varying function which represents the deviation from a plane wave. By inserting 1.2 into 1.3 and assuming that Ψ varies so slowly with z that its second derivative can be neglected, obtaining the well know parabolic approximation to the wave equation:

$$\frac{\partial^2 \Psi}{\partial x^2} + \frac{\partial^2 \Psi}{\partial y^2} - 2jk\frac{\partial \Psi}{\partial z} = 0 \tag{1.4}$$

The differential equation 1.4 for Ψ is similar to the time dependent Schrodinger equation with solution of the type:

$$\Psi = e^{-j\left(P(z)+\frac{k}{2q}r^2\right)} \tag{1.5}$$

where:

$$r^2 = x^2 + y^2 \tag{1.6}$$

The parameter $P(z)$ represents a *complex phase* shift associated to the propagation of the beam along the z axis, $q(z)$ is the *complex parameter* which describe the Gaussian beam intensity with the distance r form the z axis.

The insertion of 1.5 in 1.4, comparing terms of equal power in r, gives the relations:

$$\frac{dq}{dz} = 1 \tag{1.7}$$

$$\frac{dP}{dz} = -\frac{j}{q} \tag{1.8}$$

The integration of 1.8 yields:

$$q(z_2) = q(z_1) + z \tag{1.9}$$

which relates the intensity of two planes, the planes in z_2 and the plane in z_1.

A wave with a Gaussian intensity profile, as 1.5, is one the most important solutions of equation 1.4 ans is often called fundamental mode as showed in Fig. 1.4.

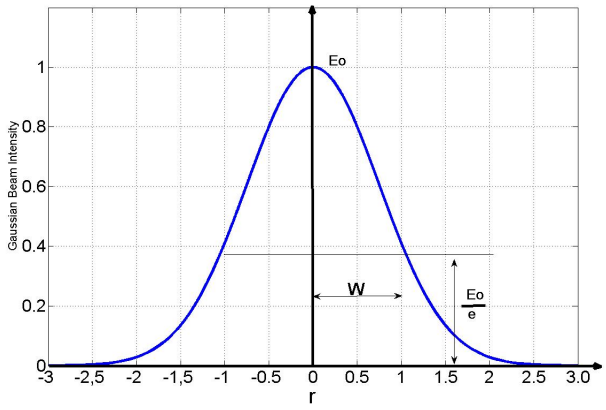

Fig. 1.4: Amplitude distribution of cavity fundamental mode

Two real beam parameter, R and ω, are introduced in relation to the complex parameters q in 1.9 by

$$\frac{1}{q} = \frac{1}{R} - j\frac{\lambda}{\pi\omega^2} \tag{1.10}$$

Introducing 1.10 in the solution 1.5, the physical meaning of $R(z)$ is the curvature radius of the wavefront that intersects the axis at z and $w(z)$ is the decrease of the field amplitude with the distance r from the axis, as showed in Fig. 1.4. The result of Ψ is:

$$\Psi = e^{-j\left(P+\frac{\pi}{\lambda}\frac{r^2}{R}\right)}e^{-\frac{r^2}{\omega^2}} \tag{1.11}$$

The parameter ω is called *beam radius* and the term 2ω the *beam diameter*. The Gaussian beam contracts to a minimum diameter $2\omega_0$ at beam waist where the phase front is plane. The beam parameter q at waist is given by:

$$q_0 = j\frac{\pi\omega_0^2}{\lambda} \tag{1.12}$$

and, using 1.9, at distance z from the waist:

$$q = q_0 + z = j\frac{\pi\omega_0}{\lambda} + z \tag{1.13}$$

Combining 1.13 and 1.11, the real and imaginary part, it gets:

$$R(z) = z\left[1 + \left(\frac{z_R}{z}\right)^2\right] \tag{1.14}$$

and

$$\omega^2(z) = \omega_0^2\left[1 + \left(\frac{z}{z_R}\right)^2\right] \tag{1.15}$$

where z_R is the Rayleigh distance:

$$z_R = \frac{\pi\omega_0^2}{\lambda} \tag{1.16}$$

The beam contour $\omega(z)$ is an hyperbola with asymptotes inclined to the axis at an angle:

$$\Theta = \frac{\lambda}{\pi\omega_0} \tag{1.17}$$

and is the far-field diffraction angle of the fundamental mode.

In 1.15 ω is the beam radius, ω_0 is the minimum beam radius (called beam waist) where one has a plane phase front at $z = 0$ and R is the curvature radius of the phase front at z. It should be noted that the phase front is not exactly spherical; therefore, its curvature radius is exactly equal to R only on the z-axis. The parameter of the Gaussian beam are illustrated in Fig. 1.5

Dividing 1.15 by 1.16, the useful relation is obtained:

$$\frac{\lambda}{\pi\omega_0^2} = \frac{\pi\omega^2}{\lambda R} \tag{1.18}$$

The expression 1.16 is used to express ω_0 and z in terms of ω and r:

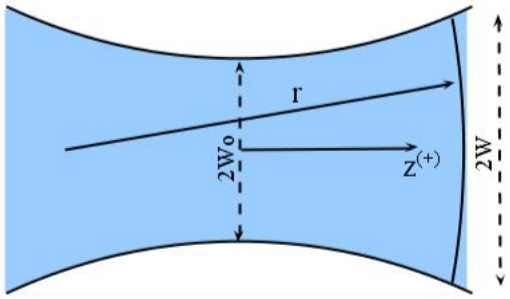

Fig. 1.5: Parameters of Gaussian Beam

$$\omega_0^2 = \frac{\omega^2}{1 + \left(\frac{\pi\omega^2}{\lambda R}\right)^2} \tag{1.19}$$

$$z = \frac{1}{1 + \left(\frac{\lambda R}{\pi\omega^2}\right)^2} \tag{1.20}$$

Inserting 1.12 in 1.8 the complex phase shift at distance z from the waist is obtained as:

$$\frac{dP}{dz} = -\frac{j}{z + j\frac{\pi\omega_0^2}{\lambda}} \tag{1.21}$$

Integration of 1.21 yields

$$jP\left(z\right) = lg\left[1 - j\left(\frac{\lambda z}{\pi\omega_0^2}\right)\right] = lg\sqrt{1 + \left(\frac{\lambda z}{\pi\omega_0^2}\right)^2} - jarctang\left(\frac{\lambda z}{\pi\omega_0^2}\right) \tag{1.22}$$

The real part of P represent the phase shift difference Φ between the Gaussian beam and an ideal wave, while the imaginary part produces an amplitude factor $\frac{\omega_0}{\omega}$ which gives the decrease of intensity due to the expansion of the beam. Then, the fundamental Gaussian beam can be written as:

$$\mu\left(r, z\right) = \frac{\omega_0}{\omega} e^{\{-j(kz-\Phi)-r^2\left(\frac{1}{\omega^2}+\frac{jk}{2R}\right)\}} \tag{1.23}$$

where

$$\Phi = arctan\left(\frac{\lambda z}{\pi\omega_0^2}\right) \tag{1.24}$$

1.5 Open Resonator Feed by Spherical Mirrors

An Open Resonator feed by two spherical mirrors (Fig. 1.6) is considered for analysis. In cartesian (x, y, z) coordinates, the separate solution for 1.4 is [7]:

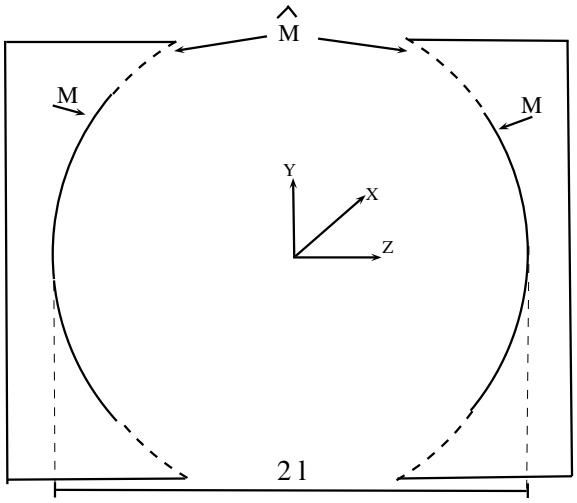

Fig. 1.6: Spherical Open Cavity

$$\Psi_{(x,y,z)} = \phi_{mp}(x, y, z)\, exp\left[j\,(m+n+1)\,tan^{-1}\frac{z}{z_R} - j\frac{\pi}{\lambda}\frac{r^2}{R(z)}\right] \tag{1.25}$$

where to have consistence with the parabolic approximation the condition $\mid m+n+1 \mid \ll (k\omega_o)^2$ must be satisfied and $\phi_{mp}(x, y, z)$ is expressed by:

$$\phi_{mp}(x, y, z) = \frac{1}{\omega(z)}\sqrt{\frac{2}{\pi 2^{m+p} m! p}} H_m\left(\sqrt{2}\frac{x}{w}\right) H_p\left(\sqrt{2}\frac{y}{w}\right) exp\left[-\frac{r^2}{w^2(z)}\right] \tag{1.26}$$

where $H_{m,p}$ are the Hermite polynomials of the rectangular mode numbers m or p.

With the assumption that the mirrors are sufficiently large to permit the total reflection of the gaussian beams of any relevant order, Ψ can be expressed as:

$$\Psi_{mpq} = u^{+}_{mpq} + u^{-}_{mpq} \tag{1.27}$$

Where u^{+}_{mpq} and u^{-}_{mpq} represent Hermite Gauss beams propagating from left to right and from right to left, respectively.

Resonance conditions depend on the mode numbers and occurs when the phase shift from one mirror to the other is a multiple of π. Using 1.3, 1.5 and 1.10 this conditions leads to :

$$k_{mpq} 2l - 2\left(m + p + 1\right) tan^{-1}\left(\frac{l}{z_R}\right) = \pi\left(q + 1\right) \tag{1.28}$$

where q is the number of nodes of the axial standing wave pattern and $2l \gg z_R$ the distance between the mirrors as showed in Fig. 1.6.

The fundamental beat frequency Δf_0 is given by:

$$\Delta f_0 = \frac{c}{4l} \tag{1.29}$$

where c is the velocity of light. From 1.11 the resonant frequency f of a mode can be expressed as:

$$\frac{f_{mpq}}{\Delta f_0} = q + 1 + \frac{1}{\pi}\left(m + p + 1\right) cos^{-1}\left(1 - \frac{2l}{R}\right) \tag{1.30}$$

1.5.1 Electromagnetic Field in the cavity

In the cavity, the expressions for the solution of scalar equation 1.4 with the boundary condition $\Phi = 0$ on the mirrors is given by:

$$\Psi_{(x,y,z)} = \phi_{mp}\left(x, y, z\right) \cos\left[k_{mpq} z - \left(m + p + 1\right) tan^{-1}\frac{z}{z_R} + \frac{\pi}{\lambda}\frac{r^2}{R\left(z\right)} + \frac{q\pi}{2}\right] \tag{1.31}$$

The electromagnetic field inside the cavity can be expressed in terms of (quasi) transverse electromagnetic modes (TEM):

$$\mathbf{E} = \sum_n V_n \mathbf{e}_n \tag{1.32}$$

$$\mathbf{H} = \sum_n I_n \mathbf{h}_n \tag{1.33}$$

Where the index n summarizes the indexes (mpq). According to the results reported in the previous section, the expressions for the $\widehat{\mathbf{y}}$ polarized modes are:

$$\mathbf{e}_n = \phi_{mp}(x,y,z)\cos\left[k_{mpq}z - (m+p+1)\,tan^{-1}\frac{z}{z_R} + \frac{\pi}{\lambda}\frac{r^2}{R(z)} + \frac{q\pi}{2}\right]\widehat{y} \tag{1.34}$$

$$\mathbf{h}_n = \phi_{mp}(x,y,z)\sin\left[k_{mpq}z - (m+p+1)\,tan^{-1}\frac{z}{z_R} + \frac{\pi}{\lambda}\frac{r^2}{R(z)} + \frac{q\pi}{2}\right]\widehat{y} \tag{1.35}$$

and similarly for the $\widehat{\mathbf{x}}$ ones

From Maxwell equations we get for the mode vectors [23]:

$$k_n\mathbf{h}_n = \nabla\times\mathbf{e}_n \tag{1.36}$$

and for the coefficients I_n, V_n

$$I_n = \frac{j\omega\varepsilon_0}{k^2-k_n^2}\frac{1}{l}\int\int_S \widehat{\mathbf{n}}\times\mathbf{E}\cdot\mathbf{h}_n^*\,dS \tag{1.37}$$

$$V_n = \frac{k_n}{k^2-k_n^2}\frac{1}{l}\int\int_S \widehat{\mathbf{n}}\times\mathbf{E}\cdot\mathbf{h}_n^*\,dS = -j\frac{\zeta_0\omega_n}{\omega}I_n \tag{1.38}$$

where S is the cavity surface and ζ_0 is the free space impedance. Note explicity that the tangential electric field appearing in expression 1.37, which, at variance with expression 1.38, does not provide a representation for the tangential components uniformly valid up to the cavity boundaries. The surface S can be divided into three parts: the coupling aperture A, the mirrors M and the (ideal) cavity boundary external to the mirrors. $\widehat{M}$ (see Fig.). Hence:

$$I_n = \frac{j\omega\varepsilon_0}{k^2-k_n^2}\frac{1}{l}\cdot\left\{\int\int_A \widehat{\mathbf{n}}\times\mathbf{E}\cdot\mathbf{h}_n^*\,dS + \int\int_M \widehat{\mathbf{n}}\times\mathbf{E}\cdot\mathbf{h}_n^*\,dS\int\int_{\widehat{M}}\widehat{\mathbf{n}}\times\mathbf{E}\cdot\mathbf{h}_n^*\,dS\right\} \tag{1.39}$$

Strictly speaking, in one of the integrals over the mirrors surfaces the coupling aperture should be deleted. However, the error introduced is negligible provided that the waveguide dimension is much smaller than that of the mirrors.

1.6 Open Resonator Feed by Rectangular Mirrors

An Open Resonator feed by two parallel metallic rectangular mirrors (Fig. 1.7) is considered for a modal analysis.

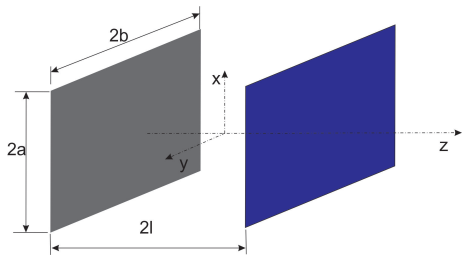

Fig. 1.7: Rectangular Open Resonator

The solution of 1.4, assuming an $e^{j\omega t}$ time dependance, can be written as

$$u = \Psi(x,y,z)e^{-jkz} - (-1)^q \Psi(x,y,-z)e^{jkz} \tag{1.40}$$

where q is the longitudinal mode number. With the boundary condition $u = 0$ in the mirrors:

$$\begin{cases} \Psi\left(x,y,-l\right) = 0, & \texttt{for } |x| > a \texttt{ or } |y| > b; \\ \Psi\left(x,y,-l\right) = e^{j(2kl-\pi q)} W\left(x,y,l\right), & \texttt{for } |x| < a \texttt{ or } |y| < b; \end{cases} \tag{1.41}$$

$$\Psi = \Psi_a\left(x,z\right)\Psi_b\left(y,z\right) \tag{1.42}$$

where the functions Ψ_a and Ψ_b satisfy the equations:

$$\frac{\partial^2 \Psi_a}{\partial x^2} - 2jk\frac{\partial \Psi_a}{\partial z} = 0 \tag{1.43}$$

$$\frac{\partial^2 \Psi_b}{\partial x^2} - 2jk\frac{\partial \Psi_b}{\partial z} = 0 \tag{1.44}$$

with the proper boundary conditions

$$\begin{cases} \Psi_a\left(x,-l\right) = 0, & \texttt{for } |x| > a; \\ \Psi_b\left(y,-l\right) = 0, & \texttt{for } |y| > b; \\ \Psi_a\left(x,-l\right) = e^{-j2\pi p_a}\Psi_a\left(x,l\right), & \texttt{for } |x| < a; \\ \Psi_b\left(y,-l\right) = e^{-j2\pi p_b}\Psi_b\left(y,l\right), & \texttt{for } |y| < b; \end{cases} \tag{1.45}$$

The eigenfrequency of the resulting mode is then given by

$$kl = \pi\left(\frac{q}{2} + p\right), \quad p = p_a + p_b \tag{1.46}$$

where

$$p_a = \frac{\pi m^2}{4\left(M_a + \beta + j\beta\right)^2}, \; m = 1, 2, ... \tag{1.47}$$

$$p_b = \frac{\pi n^2}{4\left(M_b + \beta + j\beta\right)^2}, \; n = 1, 2, ... \tag{1.48}$$

$$M_a = \sqrt{\frac{2ka^2}{l}}, \quad M_b = \sqrt{\frac{2kb^2}{l}} \tag{1.49}$$

and

$$\gamma = -\frac{\zeta_R\left(\frac{1}{2}\right)}{\sqrt{\pi}} = 0.824 \tag{1.50}$$

In (1.50) ζ_R is the Rieman's Zeta function.

We introduce the dimensionless coordinates:

$$\xi = \sqrt{\frac{k}{2l}}x, \quad \eta = \sqrt{\frac{k}{2l}}y, \quad \zeta = \frac{z}{2l} \tag{1.51}$$

In that coordinate system ξ and η assume the value

$$\xi = \pm\frac{M_a}{2}, \quad \eta = \pm\frac{M_b}{2} \tag{1.52}$$

at the end of the mirror $x = \pm a$; $y = \pm b$. The parameter $M_{a,b}$ is related to the Fresnel number N

$$M = \sqrt{8\pi N} \tag{1.53}$$

In the coordinates (ξ, η, ζ) we have

$$\Psi = f_a\left(\xi\right) f_b\left(\eta\right) e^{2\pi p\left(\zeta + \frac{1}{2}\right)} \tag{1.54}$$

where

$$f_a(\xi) = \cos\frac{\pi m\xi}{(M_a+\gamma+j\gamma)}, \quad (m=1,3...)$$
$$f_a(\xi) = \sin\frac{\pi m\xi}{(M_a+\gamma+j\gamma)}, \quad (m=2,4...)$$
$$f_b(\eta) = \cos\frac{\pi n\eta}{(M_b+\gamma+j\gamma)}, \quad (n=1,3...)$$
$$f_b(\eta) = \sin\frac{\pi n\eta}{(M_b+\gamma+j\gamma)}, \quad (n=2,4...) \tag{1.55}$$

and

$$u(\xi,\eta,\zeta) = 2e^{-j\pi p} f_a(\xi) f_b(\eta)\cos(\pi q\zeta), (\text{q even}) \tag{1.56}$$
$$u(\xi,\eta,\zeta) = 2e^{-j\pi p} f_a(\xi) f_b(\eta)\sin(\pi q\zeta), (\text{q odd}) \tag{1.57}$$

1.6.1 Electromagnetic field in the cavity

The electromagnetic field inside the cavity can be expressed in terms of (quasi) transverse electromagnetic modes

$$\mathbf{E} = \sum_{mn} V_{mn}\mathbf{e}_{mn} \tag{1.58}$$

$$\mathbf{H} = \sum_{mn} I_{mn}\mathbf{h}_{mn} \tag{1.59}$$

The relation of $u = u(x,y,z)$ to the electromagnetic field can be established with the aid of Hertz vector Π^e which determines the electromagnetic field through

$$\mathbf{e} = \nabla\nabla\cdot\Pi^2 + k^2\Pi^e \tag{1.60}$$

$$\mathbf{h} = j\frac{k}{Z_w}\nabla\times\Pi^e \tag{1.61}$$

where $k = w\sqrt{\omega\varepsilon}$ and $Z_w = \sqrt{\frac{\omega}{\varepsilon}}$. In 1.60 and 1.61 we set:

$$\Pi^e_x = u \quad \Pi^e_y = \Pi^e_z = 0 \tag{1.62}$$

neglecting the losses and considering the mode (111), we obtain the modal solution for the y component of magnetic field

$$H_y = -j\frac{k}{Z_w}\frac{\pi}{l}e^{-j\pi p} cos\left(\frac{\pi\xi}{M_a+\gamma}\right) cos\left(\frac{\pi\eta}{M_b+\gamma}\right) sin(\pi\zeta) \tag{1.63}$$

and the x component of electric field

$$E_x = \left[k^2 - \frac{k}{2l}\frac{\pi^2}{(M_a+\gamma)^2}\right]^2 2e^{-j\pi p} cos\left(\frac{\pi\xi}{M_a+\gamma}\right) cos\left(\frac{\pi\eta}{M_b+\gamma}\right) cos(\pi\zeta) \tag{1.64}$$

From 1.63 and 1.64 we obtain the equivalent surface impedance at the ascisse z

$$Z_s = jZ_w\frac{2l}{\pi}\left[k - \frac{1}{2l}\frac{\pi^2}{(M_a+\gamma)^2}\right] cot\left(\frac{\pi}{2l}z\right) \tag{1.65}$$

1.7 Cavity feed by a rectangular waveguide

A complete analysis of the coupling between the cavity and the waveguide has been done in [20] where the electromagnetic fields inside the cavity and in the waveguide are analysed and taken into account for the continuity analysis in the feeding of the cavity.

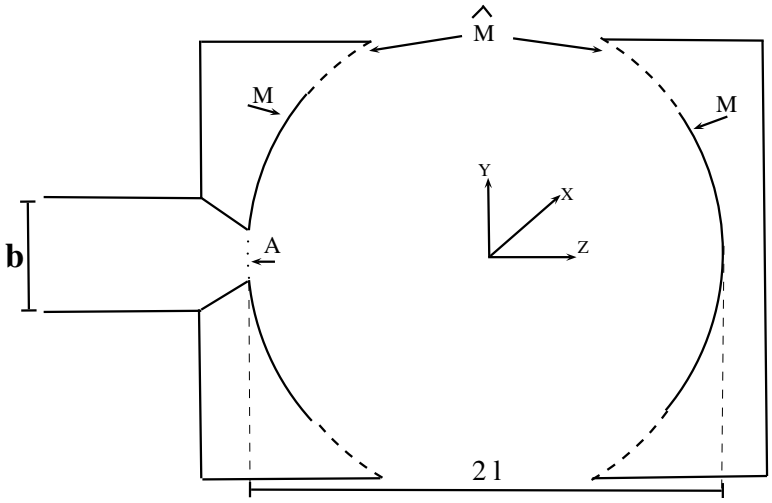

Fig. 1.8: Spherical Open Cavity feed by a rectangular waveguide

A metallic waveguide is assumed to feed the cavity. The waveguide field on the coupling aperture A is represented as:

$$\mathbf{E}^g = \sum_n V_n^g \mathbf{e}_n^g \tag{1.66}$$

$$\mathbf{H}^g = \sum_n I_n^g \mathbf{h}_n^g \tag{1.67}$$

where $\mathbf{e}^g$ and$\mathbf{h}^g$ are TE electromagnetic modes of the waveguide.

Assuming that the mirror curvature can be neglected over the extension of the coupling aperture, fields 1.66 1.67 verify the following orthonormality relation:

$$\int\int_A \mathbf{e}_n^g \times \mathbf{h}_m^g \cdot \widehat{\mathbf{z}}\, dS = \delta_{nm} \tag{1.68}$$

Expressing the field over the coupling aperture A by means of expression 1.67 we obtain from 1.2:

$$I_n + 2F_n \sum_m{}' \alpha_{nm} I_m = \frac{F_n}{\zeta_0} \sum_m \beta_{nm} V_m^g \tag{1.69}$$

where:

$$F_n = \frac{j\frac{k}{l}}{\left(k^2 - k_n^2 + \frac{kk_n}{Q_{rn}}\right) - j\frac{kk_n}{Q_{rn}}} \tag{1.70}$$

and:

$$\beta_{nm} = \int\int_A \mathbf{e}_m^g \times \mathbf{h}_n^* \cdot \widehat{\mathbf{n}}\, dS = -\int\int_A \mathbf{h}_n^* \cdot \mathbf{h}_m^g\, dS \tag{1.71}$$

By introducing the matrices $\underline{\underline{A}}$ and $\underline{\underline{B}}$, whose elements are:

$$a_{nm} = \begin{cases} \frac{1}{F_n} & n = m \\ 2\alpha_{nm} & n \neq m \end{cases} \tag{1.72}$$

and β_{nm} respectively and the vectors $\underline{I} \equiv \{I_n\}$ and $\underline{V}^g \equiv \{V_n^g\}$, relation 1.2 can be written in a compact form as:

$$\zeta_0 \underline{\underline{\mathcal{A}}} \cdot \underline{I} = \underline{\underline{\mathcal{B}}} \cdot \underline{V}^g = \underline{\underline{\mathcal{B}}} \cdot \left(\underline{V}^+ + \underline{V}^-\right) \tag{1.73}$$

wherein $\underline{V}^+$ and $\underline{V}^-$ aare the vectors of the incident and reflected waveguide mode amplitudes respectively. By enforcing the continuity of the magnetic field tangential component over the coupling aperture, we get:

$$-\underline{\underline{\mathcal{B}}}^{+} \cdot \underline{I} = \underline{I}^{g} = \frac{1}{\zeta_0} \underline{\underline{\zeta}}^{-1} \cdot \left(\underline{V}^{+} + \underline{V}^{-} \right) \tag{1.74}$$

wherein $\underline{\underline{\mathcal{B}}}^{+}$ is the adjoint of $\underline{\underline{\mathcal{B}}}$ and $\underline{\underline{\zeta}}$ is the diagonal matrix whose elements are the modes characteristic impedances normalized to ζ_0. From **??** and **??** we immediately obtain:

$$\left(\underline{\underline{\mathcal{I}}} - \underline{\underline{\mathcal{A}}}^{-1} \cdot \underline{\underline{\mathcal{B}}} \cdot \underline{\underline{\zeta}} \cdot \underline{\underline{\mathcal{B}}}^{+} \right) \cdot \underline{I} = \frac{2}{\zeta_0} \underline{\underline{\mathcal{A}}}^{-1} \cdot \underline{\underline{\mathcal{B}}} \cdot \underline{V}^{+} \tag{1.75}$$

$$\left(\underline{\underline{\mathcal{I}}} - \underline{\underline{\zeta}} \cdot \underline{\underline{\mathcal{B}}}^{+} \cdot \underline{\underline{\mathcal{A}}}^{-1} \cdot \underline{\underline{\mathcal{B}}} \right) \cdot \underline{V}^{-} = \left(\underline{\underline{\mathcal{I}}} + \underline{\underline{\zeta}} \cdot \underline{\underline{\mathcal{B}}}^{+} \cdot \underline{\underline{\mathcal{A}}}^{-1} \cdot \underline{\underline{\mathcal{B}}} \right) \cdot \underline{V}^{+} \tag{1.76}$$

wherein $\underline{\underline{\mathcal{I}}}$ is the unit matrix and $\underline{\underline{\mathcal{A}}}^{-1}$ the inverse of the matrix $\underline{\underline{\mathcal{A}}}$.

Solution of eq.1.75 and 1.76 provides the answer of the problem. In particular, from 1.76 the (formal) expression for the feeding waveguide scattering matrix $\mathcal{S}$ becomes:

$$\underline{\underline{\mathcal{S}}} = \left(\underline{\underline{\mathcal{I}}} - \underline{\underline{\zeta}} \cdot \underline{\underline{\mathcal{B}}}^{+} \cdot \underline{\underline{\mathcal{A}}}^{-1} \cdot \underline{\underline{\mathcal{B}}} \right)^{-1} \cdot \left(\underline{\underline{\mathcal{I}}} + \underline{\underline{\zeta}} \cdot \underline{\underline{\mathcal{B}}}^{+} \cdot \underline{\underline{\mathcal{A}}}^{-1} \cdot \underline{\underline{\mathcal{B}}} \right) \tag{1.77}$$

1.7.1 Field on the coupling aperture

In order to solve the system (1.75 -1.76)a suitable description of the field on the aperture A is necessary. Any device, able to support electromagnetic field matching the cavity field on the mirror (1.32 - 1.33), can be used to feed the cavity.

A rectangular metallic waveguide, with transverse $a \times b$, is assumed to feed the cavity. The waveguide TE electromagnetic modes of the metallic rectangular waveguide, on the coupling aperture A, is represented as:

$$\mathbf{h}_n = \mathbf{h}_{pq} = \frac{1}{k_{tpq}} \sqrt{\frac{4\varepsilon_p \varepsilon_q}{ab}} \cdot \left\{ \frac{p\pi}{a} sin\frac{p\pi}{a} \left(x + \frac{a}{2} \right) cos\frac{q\pi}{b} \left(y + \frac{b}{2} \right) \widehat{\mathbf{x}} + \frac{q\pi}{b} cos\frac{p\pi}{a} \left(x + \frac{a}{2} \right) sin\frac{q\pi}{b} \left(y + \frac{b}{2} \right) \widehat{\mathbf{y}} \right\} \tag{1.78}$$

$$\mathbf{e}_{pq} = \mathbf{h}_{pq} \times \widehat{\mathbf{z}} \tag{1.79}$$

$$\varepsilon_p = \{1, \quad p \neq 0; \frac{1}{2}, \quad p = 0 \tag{1.80}$$

$$k_{tpq}^2 = \left(\frac{p\pi}{a}\right)^2 + \left(\frac{q\pi}{b}\right)^2 \tag{1.81}$$

and the TM electromagnetic modes:

$$\mathbf{e}_n = \mathbf{e}_{pq} = -\frac{1}{k_{tpq}}\sqrt{\frac{4\varepsilon_p\varepsilon_q}{ab}}\cdot \left\{\frac{p\pi}{a}cos\frac{p\pi}{a}\left(x+\frac{a}{2}\right)sin\frac{q\pi}{b}\left(y+\frac{b}{2}\right)\widehat{\mathbf{x}} + \frac{q\pi}{b}sin\frac{p\pi}{a}\left(x+\frac{a}{2}\right)cos\frac{q\pi}{b}\left(y+\frac{b}{2}\right)\widehat{\mathbf{y}}\right\} \tag{1.82}$$

$$\mathbf{h}_{pq} = \widehat{\mathbf{z}} \times \mathbf{e}_{pq} \tag{1.83}$$

Note explicitly that in expressions (1.78 - **??**) the index n summarizes the indexes (pq).

1.7.2 Equivalent Circuit

Let us to consider systems 1.75 and 1.76 under the following assumption:

1. Negligible intercoupling between cavity modes, i.e. :

$$\left(\underline{\underline{A}}\right)_{pq} = \frac{1}{F_p}\delta_{pq} \Longleftrightarrow \left(\underline{\underline{A}}^{-1}\right)_{pq} + F_p\delta_{pq} \tag{1.84}$$

2. Single cavity mode approximation, i.e.:

$$F_p = \delta_{p0}F_0 \tag{1.85}$$

3. Beam diameter at the mirror much larger than the waveguide dimension, i.e.:

$$\omega = \omega\left(l\right) \gg a \tag{1.86}$$

Putting

$$V_n^g = V_1^+\delta_{1n} + V_n^- \tag{1.87}$$

and taking(1.84 -1.86) into account, equation (1.75 -1.76) became

$$-\zeta_0\zeta_n\beta_{0n}I_0 = V_1^+\delta_{0n} - V_n^- \tag{1.88}$$

$$\left(1 - F_0 \sum_k \beta_{0k}^2 \zeta_k\right) I_0 = 2\frac{F_0}{\zeta_0}\beta_{01} V_1^+ \tag{1.89}$$

From 1.88 and 1.89 V_n is expressed as:

$$V_n^- = \left(\delta_{1n} + \frac{2F_0\zeta_n \frac{\beta_{0n}}{\beta_{01}}}{1 - F_0 \sum_k \beta_{0k}^2 \zeta_k}\right) V_1^+ \tag{1.90}$$

Hence

$$\Gamma = \frac{V_1^-}{V_1^+} = \frac{1 + F_0\zeta_1\beta_{01}^2 - F_0 \sum_{k\neq 1} \beta_{0k}^2 \zeta_k}{1 - F_0 \sum_k \beta_{0k}^2 \zeta_k} \tag{1.91}$$

From 1.91 the equivalent terminal impedance relative to the fundamental mode is:

$$Z = \beta_0\beta_1 \frac{1+\Gamma}{1-\Gamma} = -\frac{\zeta_0}{\beta_{01}^2 F_0} + \zeta_0 \sum_{k\neq 1} \frac{\beta_{0k}}{\beta_{01}}^2 \zeta_k \tag{1.92}$$

Taking into account for the expression 1.70 for F_0, Fig. 1.8 shows the equivalent circuit.

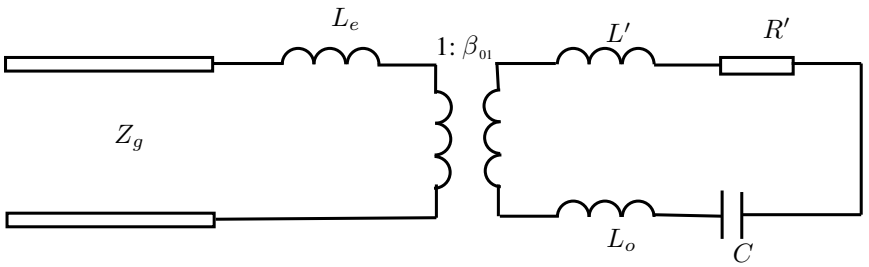

Fig. 1.9: Equivalent circuit of open cavity coupled to a feeding waveguide.

where the explicit expression for its elements are collected under Table 1.1.

The value of L_e depends on the feeding waveguide and is reported in the following subsection for rectangular waveguide.

Table 1.1: Expression for the Equivalent Circuit Elements of Fig. 1.8

L_o	$\mu_o l(H)$	C	$\frac{\epsilon l}{(\kappa_o l)^2}(F)$
L'	$\mu_o \delta(H)$	R'	$\frac{2}{\sigma\delta}(\Omega)$

The cavity is assumed to be excited by the incident fundamental TE_{10} mode. From expressions 1.66, 1.67 and 1.78 follows than the cavity are excited only the $(0,0,q)$ mode, in the feeding waveguide are excited the modes TE_{n0}

When the cavity is fed by a rectangular waveguide under the approximation 3), the expression 1.71 for β_{0k} can be explicitly evaluated, leading to:

$$\beta_{0n} = \frac{4}{pi}\frac{1}{n}\sqrt{\frac{ab}{\omega^2}} \quad n = 1, 3, \cdots \tag{1.93}$$

Hence, for the sum at the right hand side of 1.92:

$$\begin{aligned} &\zeta_0 \sum_{k=3,5,\cdots} \left(\frac{\beta_{0k}}{\beta_{01}}\right)^2 \zeta_k = j\zeta_0 \sum_{k=0}^{\infty} \frac{1}{(2k+3)^2} \frac{1}{\sqrt{\left(\frac{2k+3}{2a}\lambda\right)^2 - 1}} \simeq \\ &j\zeta_0 \left(\frac{2a}{\lambda}\right) \sum_{k=0}^{\infty} \frac{1}{(2k+3)^2} = j\omega\mu a \frac{1}{pi}\left[\left(1 - \frac{1}{8}\right)\zeta\{3\} - 1\right] = j\omega L_e \end{aligned} \tag{1.94}$$

wherein $\zeta.$ denotes the Rieman zeta function. From equation 1.94, the value of L_e is:

$$L_e = 16.510^{-3}\mu_0 a\,[henry] \tag{1.95}$$

2

Extraction of Equivalent Electrical Model for Measuring of Permittivity of Dielectric Material

2.1 Introduction

Low loss dielectric materials are widely used for the design of microwave and millimetre-wave circuits components and antennas. With the increasing demand for improved system performances and the adoption of new dielectric materials [24], the electromagnetic characterization of dielectric substrates ([25]-[28]) has become a fundamental task.

The use of open resonators either in the microwave region or at higher frequencies (optical region) has taken place over a number of decades. The related theory and its applications has found a widespread use in several branches of optical physics and today is incorporated in many scientific instruments [29].

In the microwave region, open resonators have also been proposed as cavities for quasi-optical gyrotrons [11] and adopted as open cavities in a plasma beat wave accelerator experiment [12]. For microwave applications, a reliable description of the coupling between the cavity and the feeding waveguide is strictly necessary.

Several papers deal with the coupling through a small hole or a rectangular waveguide by taking into account only the fundamental cavity and waveguide modes ([17]-[19]).

In [20], a complete analysis of the coupling between a rectangular waveguide and an open cavity has been developed by taking into account all the relevant eigenfunctions into the waveguide as well as into the cavity.

Starting from the theoretical foundation of the open resonator method for dielectric characterization [[30]-[32]], several papers have been written concerning the use of open resonator as a convenient tool for measuring the complex permittivity of a dielectric material [[33]-[40]].

They all start from the expression derived from Yu and Cullen [30], assuming an ideal open cavity.

In this chapter, an improved open resonator technique for dielectric characterization is proposed. An open cavity fed by a rectangular waveguide is adopted, with a transition specifically designed to optimize the coupling on the basis of a complete modal expansion analysis as developed in [20]. The equivalent circuit of the open resonator system originally proposed in [20] is extended in this work to include the inserted dielectric sample. Starting from the results in [20], where the coupling between an empty cavity and a rectangular waveguide is accurately characterized in terms of a full modal expansion in both devices, the equivalent circuit proposed in [20] is properly extended to include the planar grounded dielectric sample, so providing a simple and eficient tool to retrieve the unknown complex permittivity from a single return loss measurement. As a matter of fact, the traditional open resonator method generally requires measurement data on more samples with different thickness's, as the unknown permittivity value must be retrieved from a transcendental equation having multiple roots [40]. As a further accuracy feature of the proposed method, a proper characterization of the gaussian beam impinging on the unknown dielectric sheet is performed to derive an accurate formulation of the waveguide input impedance as a function of the complex dielectric permittivity, which is accurately retrieved from return loss measurements. When compared to the approach proposed in [30], the following significant improvements are introduced:

- losses due to the non ideal mirror conductivity are properly taken into account;
- the frequency shift due to the cavity enlargement which is caused by the electromagnetic field penetration into the cavity walls is specially modelled;
- additional reactances are introduced in the equivalent circuit to model the coupling between the cavity and the higher order modes of the feeding waveguide.

The proposed method is successfully tested on thin grounded dielectric substrates usually adopted in the design of microwave planar circuits and antennas.

2.2 Open Resonator Technique

The case of a rectangular waveguide coupled with an open cavity has been studied in details [20], confirming that the coupling between cavity modes is negligible and that the single resonant mode approximation gives a good description of the cavity field as only this last mode is practically excited. At the same time, the analysis of the solutions has also demonstrated that the excitation of higher order waveguide modes TE_{n0} is important for the accurate coupling description.

The equivalent circuit adopted in [20] to accurately model a cavity coupled to a feeding waveguide is illustrated under 2.1. The explicit expressions of the circuit elements as a function of the cavity and the waveguide parameters are reported under Table 2.1. In particular, the component R' models the losses due to the finite conductivity of the mirrors, while L' represents the effect of the skin depth δ. It sums to the inductive circuit part L_o o modelling the cavity, thus producing a shift in the resonant frequency, which is equivalent to a cavity enlargement.

Here, $2l$ gives the cavity length, a is the major waveguide dimension, σ represents the conductivity, while $\kappa_o = \frac{2\pi f_o}{c}$ is the wave number of free space, c being the velocity of light and f_o the resonant frequency of the empty resonator. The circuit element Z_g appearing into 2.1 represents the characteristic impedance of the transmission line equivalent to the excited fundamental mode of the feeding waveguide.

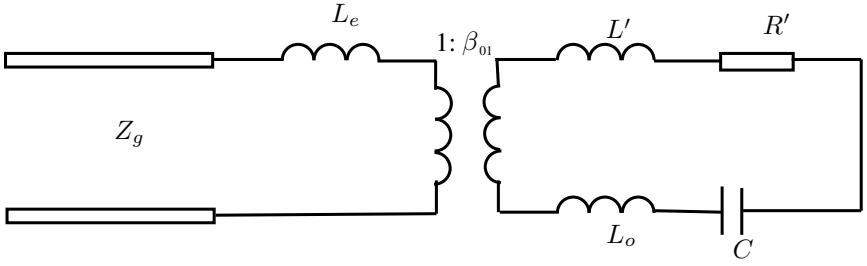

Fig. 2.1: Equivalent circuit of open cavity coupled to a feeding waveguide.

From the circuit reported under 2.1 is straightforward to deduce the waveguide input impedance Z_i and the reflection coefficient Γ, respectively given as:

$$Z_i = j\omega L_e + \frac{Z_R}{{\beta_{01}}^2} \tag{2.1}$$

Table 2.1: Expression for the Equivalent Circuit Elements under 2.1

L_o	$\mu_o l(H)$	C	$\frac{el}{(\kappa_o l)^2}(F)$
L'	$\mu_o \delta(H)$	R'	$\frac{2}{\sigma\delta}(\Omega)$
L_e	$16.5 \times 10^{-3}\mu_o a(H)$		

$$\Gamma = \frac{Z_i^{cc} - Z_{10}}{Z_i^{cc} + Z_{10}} \tag{2.2}$$

Where:

$$Z_R = j\omega L_T + R' + \frac{1}{j\omega C} \tag{2.3}$$

$$L_T = L_o + L' \tag{2.4}$$

while β_{01} is the waveguide cavity factor as reported in [12].

In order to test the validity of the proposed approach, the results of a complete modal analysis, as developed in [20], which assumes a relevant number of modes both in the feeding waveguide and into the cavity, are compared with those obtained from the adopted equivalent circuit. No significant difference is observed from the comparison, thus implying the possibility to use a simple circuit analysis tool, instead of the complete modal approach, in many practical cases.

2.3 Design and Optimization Based on the Equivalent Circuit Model

The insertion of the unknown planar sample into the open cavity gives the system depicted under 2.2, with the equivalent circuit modified as in 2.4 through the addition of the impedance Z_ϵ due to the grounded dielectric material:

$$Z_\epsilon = jZ_d \tan\left[\kappa_d h - \Phi_G\right] \tag{2.5}$$

The terms Z_d and κ_d into 2.5 give the characteristic impedance and the propagation constant of the unknown dielectric, respectively, while the phase shift Φ_G takes into account for the Gaussian nature of the beam, and is given as [17]:

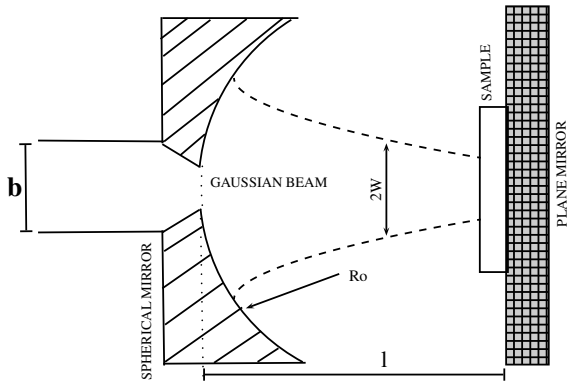

Fig. 2.2: Hemispherical open resonator system for dielectric characterization

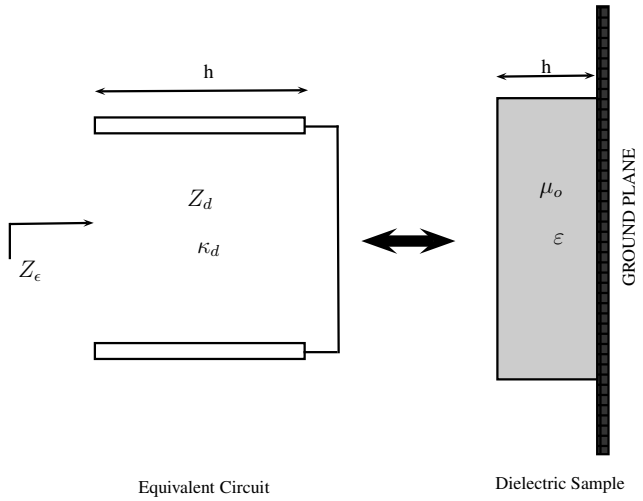

Fig. 2.3: Equivalent Circuit for a dielectric sample with a ground plane

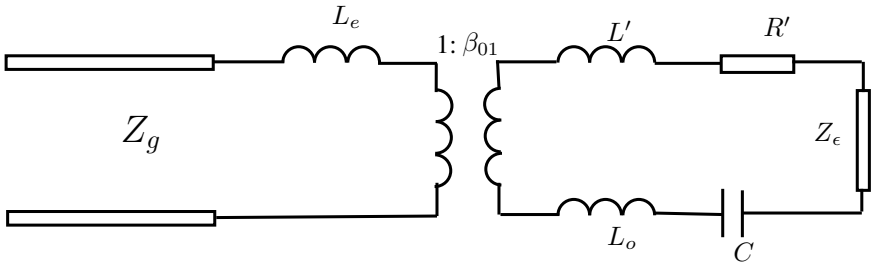

Fig. 2.4: Equivalent circuit relative to the open resonator system of 2.2

$$\Phi_G = \arctan \frac{h}{Z_R} \tag{2.6}$$

where $Z_R = \sqrt{Rl - l^2}$ is the Rayleigh distance.

Due to the negligible contribution of the Gaussian amplitude variation, a uniform wave has been assumed, leading to use an equivalent circuit approach, while the phase term Φ_G introduced by the Gaussian wave is properly considered to model the associated resonant frequency shift.

When assuming a complex dielectric constant $\varepsilon = \varepsilon' - j\varepsilon'' = \varepsilon\{1 - j\tan\delta\}$ for the unknown sample, it is easy to obtain:

$$Z_\epsilon = j\frac{Z_o}{a_\epsilon\left(1 - jb_\epsilon\right)}\tan\left\{\kappa_o\left[a_\epsilon\left(1 - jb_\epsilon\right)h\right] - \Phi_G\right\} \tag{2.7}$$

where $a_\epsilon = \sqrt{\varepsilon'}$ and $b_\epsilon = \frac{1}{2}\tan\delta$

It is useful to express the impedance Z_ϵ in terms of its real and imaginary parts, namely:

$$Re\left[Z_\epsilon\right] = \frac{Z_o}{a_\epsilon\left({b_\epsilon}^2 + 1\right)}\frac{\sinh\left(2a_\epsilon b_\epsilon h\kappa_o\right) - b_\epsilon\sin\left[2\left(a_\epsilon h\kappa_o + \arctan\frac{\lambda h}{\pi{\omega_o}^2}\right)\right]}{\cosh\left(2a_\epsilon b_\epsilon h\kappa_o\right) + \cos\left[2\left(a_\epsilon h\kappa_o + \arctan\frac{\lambda h}{\pi{\omega_o}^2}\right)\right]} \tag{2.8}$$

$$Im\left[Z_\epsilon\right] = \frac{Z_o}{a_\epsilon\left({b_\epsilon}^2 + 1\right)}\frac{b_\epsilon\sinh\left(2a_\epsilon b_\epsilon h\kappa_o\right) + \sin\left[2\left(a_\epsilon h\kappa_o + \arctan\frac{\lambda h}{\pi{\omega_o}^2}\right)\right]}{\cosh\left(2a_\epsilon b_\epsilon h\kappa_o\right) + \cos\left[2\left(a_\epsilon h\kappa_o + \arctan\frac{\lambda h}{\pi{\omega_o}^2}\right)\right]} \tag{2.9}$$

Equations 2.8 and 2.9 can be easily applied to obtain the waveguide input impedance, given as:

$$Z_i = \frac{R' + Re\left[Z_\epsilon\right]}{\beta_{01}^2} + j\omega L_e + \frac{j\omega L_T + \frac{1}{j\omega C} + jIm\left[Z_\epsilon\right]}{\beta_{01}^2} \tag{2.10}$$

The imaginary part of the impedance Z_ϵ gives a shift in the resonant frequency of the cavity, while its real part produces an amplitude reduction of the reflection coefficient at the cavity input. The measurement of the above shift and amplitude can be in principle combined to retrieve the unknown complex permittivity $\varepsilon' - j\varepsilon''$. However, due to the high quality factor Q of the cavity, that means a very narrow resonant bandwidth, it is very difficult to measure the exact value of the reflection coefficient and consequently the dielectric loss. A high Q value gives, in principle, an advantageous feature,

however it implies a reduced frequency range and so a strong sensitivity of the measurement accuracy to slight changes of the test setup, due also to the finite resolution of the network analyser.

In alternative way, we can use the information relative to the resonant frequencies of the empty and dielectric loaded cavity, respectively equal to f_o and f_R , to determine the imaginary part of Z_ϵ . As a second step, we can use the information relative to the loaded dielectric quality factor Q_L , which is inversely proportional to the difference between the 3 dB frequencies f_1 , f_2 at each side of the resonance minimum, namely:

$$Q_L = \frac{f_o}{f_2 - f_1} \tag{2.11}$$

The knowledge of the term Q_L leads to retrieve the dissipation factor into the open resonator, from which the real part of expression 2.10, and consequently the real part of impedance Z_ϵ can be obtained. Finally, from the conjuncted knowledge of $Re\,[Z_\epsilon]$ and $Im\,[Z_\epsilon]$, the terms a_ϵ and b_ϵ can be retrieved, which are related to the real and imaginary parts of the unknown complex permittivity.

The numerical implementation of the method described above is performed by a two step procedure. First, the imaginary part ε'' of the permittivity is neglected and 2.9 is solved with respect to the variable a_ϵ, directly related to the real part ε' . This computed value is then inserted into 2.8 to obtain the term b_ϵ , which is in turns related to the unknown dielectric loss tangent.

2.4 Experimental Results

In order to test the validity of the proposed approach, a $K - band$ open resonator fed by a WR62 rectangular waveguide is designed and realized (Fig. 2.5).

Table 2.2: Nominal parameters of tested dielectric substrates

n	Material	Thickness (mm)	ε' (10 GHz)	$\tan\delta$ (10 (GHz)
1	AR600L03111	0,762	6,00	0.0030
2	Diclad527B0301155	0,762	2,55	0.0018
3	Diclad25FR030011	0,762	3,58	0,0035

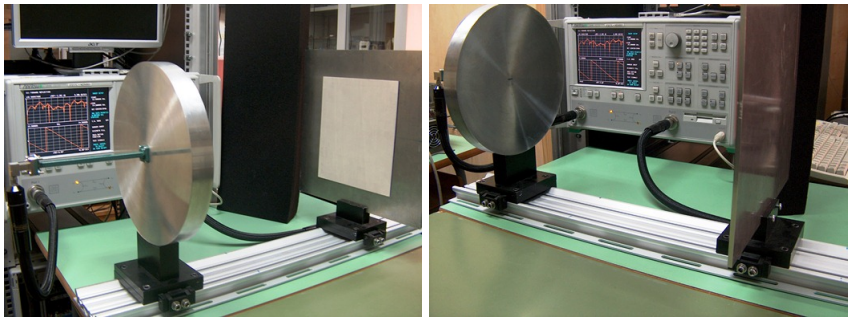

Fig. 2.5: Photograph of realized K-band open resonator system

The theory outlined in the previous section is applied to accurately determine the dimension of the waveguide to cavity transition on the basis of the coupling optimization. At this purpose, a parametric analysis of the reflection coefficient at the waveguide input is performed in terms of the waveguide height b, for a fixed design frequency $f_o = 24GHz$, thus deriving the curve reported in Fig. 2.6. Due to the mechanical tolerances of the available machine, a value equal to 0.7 mm, slightly larger than that giving the minimum reflection coefficient, is adopted for the smaller height of the transition, starting from the standard WR62 value $b = 4.3mm$.

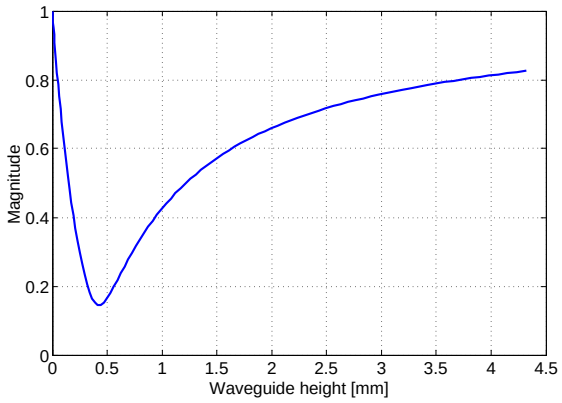

Fig. 2.6: Reflection Coefficient at the waveguide input versus waveguide height

The open resonator is designed on aluminium material, by assuming a radius $R_0 = 517mm$ and a distance $l = 490mm$ between the mirrors, this latter giving the excitation of a $TEM_{0,0,76}$ mode inside the cavity. The open resonator radius, the longitudinal mode number and the relative length l are

derived from a compromise choice on the basis of the following parameters:
(i) the fixed working frequency;
(ii) the resonator stability;
(iii) a proper waist on the mirror which avoids diffraction losses;
(iv) a waist value on the sample greater than a wavelength in order to measure the diffraction features of resonant objects.

In order to test the proposed approach, three different dielectric substrates, usually adopted for the realization of microwave planar circuits, are considered. The nominal parameters of the tested dielectrics as available from the producer are reported in Table 2.2.

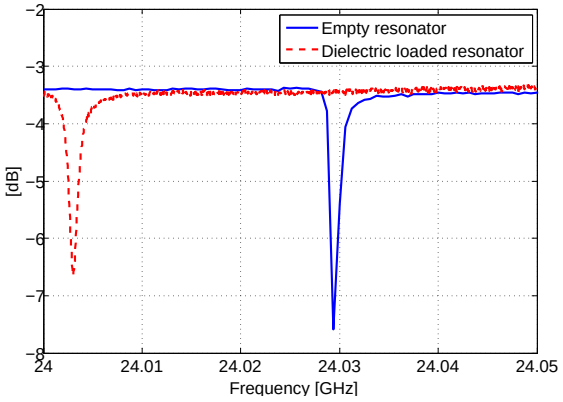

Fig. 2.7: Measured return loss for test material n. 1 (Comparison between empty and loaded cavity cases)

The measured return loss curves obtained in the presence of empty and loaded cavity of Fig. 2.5 are compared in Figs. 2.7-2.9 for the three tested dielectrics of Table 2.2. In all cases, a frequency shift together with an amplitude reduction of the return loss can be observed when inserting the dielectric sample.

In order to retrieve the unknown complex permittivity for the dielectric samples, the theory outlined in the previous section is properly applied by measuring the frequency shift $\Delta f = f_R - f_0$ and the 3 dB frequencies f_1 , f_2 at each side of the resonant frequency f_L, which give the quality factor Q_L . These measured quantities are reported in Table 2.3, where the values of ε' and $\tan\delta$ as retrieved from expressions 2.8 and 2.9 are also indicated.

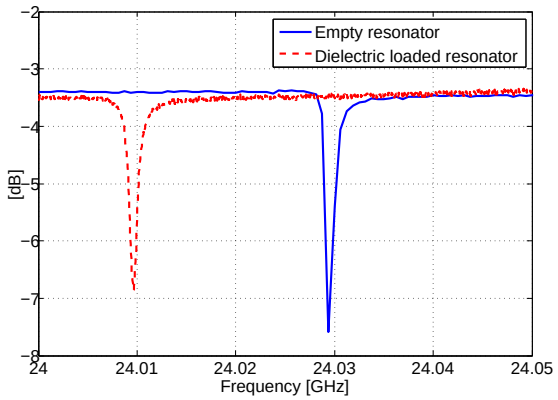

Fig. 2.8: Measured return loss for test material n. 2 (Comparison between empty and loaded cavity cases)

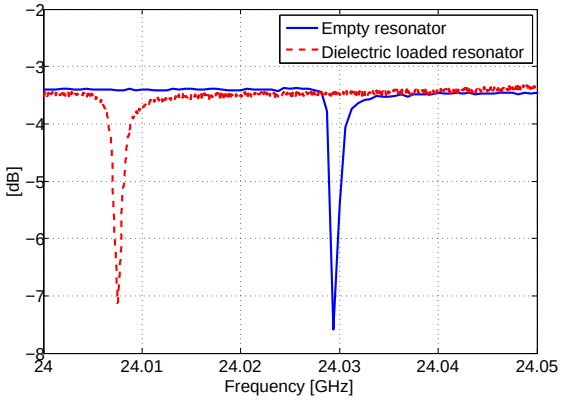

Fig. 2.9: Measured return loss for test material n. 3 (Comparison between empty and loaded cavity cases)

The effectiveness of the approach is further demonstrated by reporting the behaviour of the resonant frequency as a function of the dielectric thickness for the three dielectric samples (Figs. 2.10-2.12). In particular, an excellent agreement between the measured data and the theoretical curve for the loaded cavity can be observed, thus demonstrating that the measured frequency shift properly corresponds to the correct dielectric thickness for all tested cases.

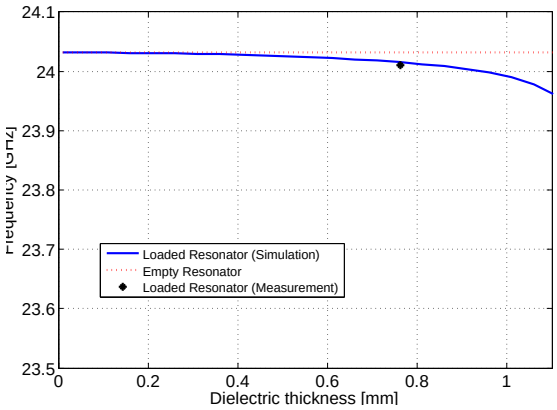

Fig. 2.10: Resonant frequency as a function of dielectric thickness for test material n.1.

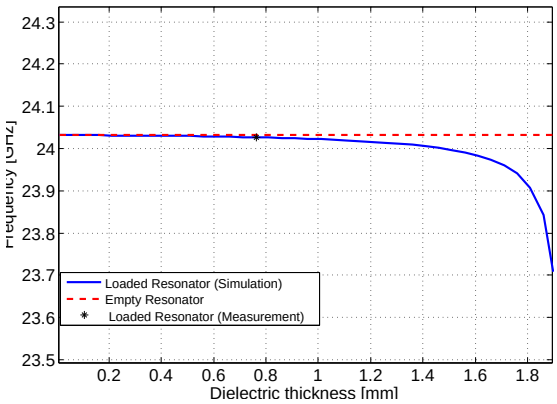

Fig. 2.11: Resonant frequency as a function of dielectric thickness for test material n.2.

Table 2.3: Measured parameters and retrieved permittivity values.

n	$f_L[GHz]$	$f_1[GHz]$	$f_2[GHz]$	$\Delta f[MHz]$	Q_L	ε'	$\tan\delta$
1	24.003	24.0018	24.0045	2.7	8890	6.00	0.00324
2	24.00965	24.00918	24.00995	0.77	31181	2.535	0.002
3	24.00752	24.00698	24.0084	1.42	16907	3.54	0.004

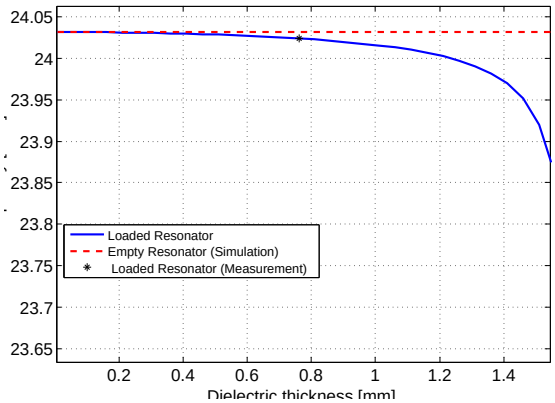

Fig. 2.12: Resonant frequency as a function of dielectric thickness for test material n.3.

3

Microstrip reflectarray elements characterization by an Open Resonator

3.1 Introduction

A microstrip reflectarray antenna consists of an array of microstrip patch elements and its concept is based on the scattering properties of these patches, traditionally passive with low-profile reflector [42]-[47]. Reflectarray antennas are designed for discrete phase manipulation at each individual antenna element making up the array and appeal all the microstrip technology features, such as less weight, easy manufacturing, and low cost, so revealing useful in many application fields such a remote sensing, millimetre wave [48], and infrared frequencies [49] .

Many different phase tuning methods have been introduced for microstrip reflectarray antennas as variable size microstrip patches [50], variable size dipoles and identical patches elements having variable length phase delay lines with or without angular rotations [[51], [52]]. Recently, new methods have been modelled where the phase-tunable elements have been considered to give reflectarray with a steerable main beam [53]-[55] and combined with dedicated electronic control system [56], [57].

Several methods have been used to design reflectarray antennas based on the use of a design curve relating the phase of re-radiated field. The analysis referred to the field scattered by a periodic array of identical elements on which transverse electromagnetic wave is normally incident is the method of primary importance. As a matter of fact, the behaviour of the reflected phase versus frequency and/or tuning element variation is used as design curve in the synthesis algorithm [58] to properly choose those elements that are able to give the prescribed reflectarray beam features.

A well-established technique for the measurement of phased-array antenna is through waveguide technology [59], where, an equivalent waveguide approach is proposed for reflectarray of variable size patches, with the unit cell

enclosed in a rectangular waveguide having perfect electric and magnetics walls [60], [61].

In [62], [63], an equivalent electrical circuit is adopted for the reflectarray, in order to derive the input reflection coefficient. In [62], the reflected phase is directly computed form the input reflection coefficient assuming a wave plane at the interface between the substrate and the air transmission layers. The equivalent circuit is the parallel circuit between the patch impedance and a transmission line ended in a short circuit. In [63], a resonant LC parallel circuit is adopted to model the reflectarray unit cell. Losses are taken into account by placing a resistor in series with the capacitor. In [64] the equivalent circuit is extended to two resonant LC series circuits that consider two resonant and two antiresonance frequencies

In this section, an open resonator system [1] with an optimized design of the waveguide-to-cavity transition [20] is proposed to characterize the reflection coefficient response of variable size reflectarray patch elements. The open resonators theory is explained in the first chapter.

3.2 Microstrip reflectarray elements characterization

Synthesis procedures for the reflectarray design [56] require the accurate phase characterization of the field reflected by the single radiating element, to properly choice the dimensions and distributions of the grid radiators giving a radiated field with prescribed featured. An array grid with identical radiating elements showed in Fig. 3.1 is analysed to characterize the single radiating element in the reflectarray antenna.

The printed reflectarray antenna can be modelled and analysed as a grounded reflecting surface by the equivalent electrical circuit of Fig. 3.2 where the relative parameters L_1, C_1 representing the grid depend on the variable length d of the reflectarray patches as well as on the grid spacing between adjacent elements, the dielectric slab is modelled as a simple transmission line with length equal to the dielectric thickness ended in a short circuit that represents the ground plane effect.

The input impedance Z_ϵ of the transmission line that express the ground plane and the dielectric effect is written as:

$$Z_\epsilon = jZ_d \tan(\beta_d h) \tag{3.1}$$

Where,

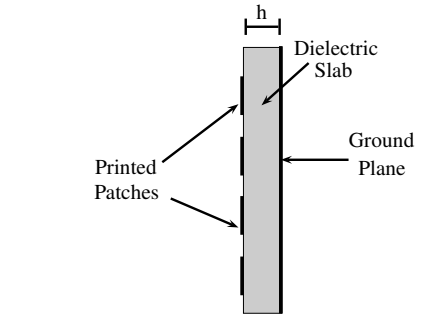

(a) Side View

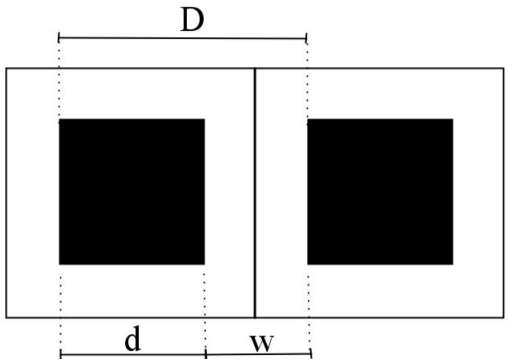

(b) Frontal View

Fig. 3.1: Reflectarray Antenna (a) Side view, (b) Frontal view

$$\beta_d = \kappa_o \sqrt{\varepsilon'}$$
$$Z_d = \frac{Z_o}{\sqrt{\varepsilon'}}$$

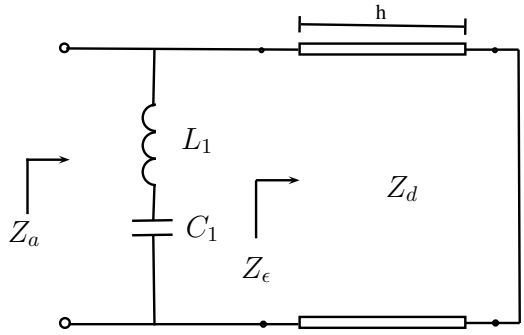

Fig. 3.2: Equivalent Circuit for a Printed Reflectarray Antenna

Where κ_o is the propagation constant, ε' is the relative permittivity of the dielectric and Z_o is the impedance in the free space.

To obtain the values of the component L_1 and C_1 is necessary to understand how the antenna works in terms of resonance frequencies and the phase of the reflection coefficient. There are necessary to consider two analysis:

- The input impedance is infinite (Reflection coefficient is 1) and it occurs in the reflectarray resonance frequency.
- The input impedance becomes zero (Reflection coefficient is -1).

The first analysis, when the reflection coefficient module is 1 but the angle is 0°, occurs when:

$$\frac{1}{j\omega L_1 + \frac{1}{j\omega C_1}} + Y_\epsilon = 0, \qquad |\Gamma| = 1, \Phi_\Gamma = 0^\circ \tag{3.2}$$

When L_1C_1 circuit becomes a short circuit, the reflection coefficient module is 1, but the angle is 180°, and it happens when:

$$j\omega L_1 + \frac{1}{j\omega C_1} = 0, \qquad |\Gamma| = 1, \Phi_\Gamma = 0^\circ(\pi \quad rad) \tag{3.3}$$

One simulation at 24 GHz has been done with this approach and the results were compared with MoM analysis using ANSOFT DESIGNER software. The results are showed in Fig. 3.3. The resonance frequencies were assumed known based in the relation between the resonance frequencies and the dimensions of the single element and the dielectric properties.

3.2.1 Reflectarray Antenna Equivalent Circuit Without Losses

Due to the small thickness h of the usually adopted substrates (typically less than a quarter wavelength), and assuming neglecting losses in the dielectric support, an equivalent inductance L_μ can be considered to model the slab ended with the ground plane. The input impedance Z_ϵ can be written as:

$$Z_\epsilon = jZ_d\beta_d h \tag{3.4}$$

but, because $\beta = \omega_o\sqrt{\mu_o\varepsilon_o\varepsilon'}$ and $Z_d = \sqrt{\frac{\mu_o}{\varepsilon_o\varepsilon'}}$, then:

$$Z_\epsilon = j\omega_o\mu_o h \tag{3.5}$$

Then, the inductance can be written as $L_u = \mu_o h$ and replaces the transmission line ended in a short circuit. The final circuit is showed in Fig. 3.4 and

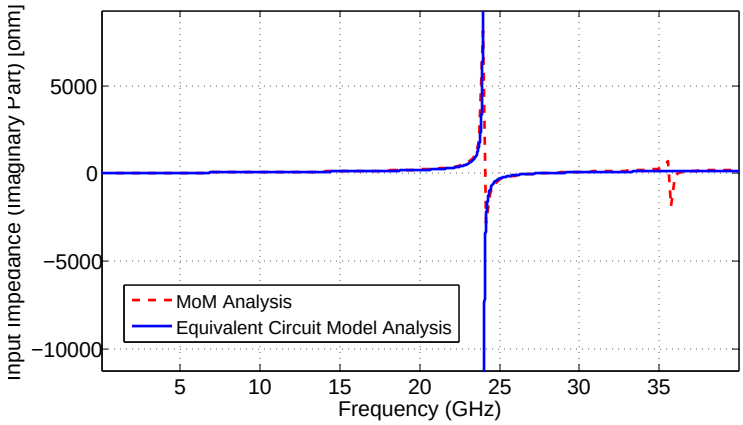

(a) Input Impedance (Imaginary part)

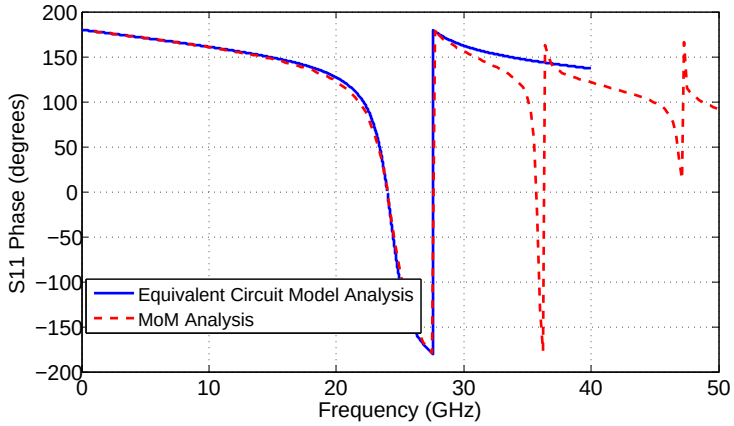

(b) Reflection Coefficient (Phase)

Fig. 3.3: Reflectarray analysis with one resonance circuit LC at 24 GHz (a) Input Impedance (Imaginary Part), (b)Reflection Coefficient (Phase)

the input impedance is purely reactive that represent no losses and a circuit that changes the resonance frequency through the variations of its components.

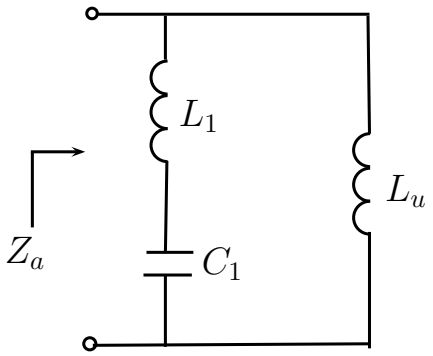

Fig. 3.4: Simplified Equivalent Circuit for a Printed Reflectarray Antenna without losses

The input impedance Z_a is:

$$Z_a = j\frac{\omega L_u\left(1-\omega^2 L_1 C_1\right)}{(1-\omega^2(L_1+L_u)C_1)} \tag{3.6}$$

3.2.2 Reflectarray Antenna Equivalent Circuit considering Losses

In the previous part, a simple analysis was done where the losses weren't considered. In this part, a complete analysis is done, then, the printed reflectarray antenna showed in Fig. 3.5 considers in plus: the dielectric losses and the dispersion losses in the propagation.

The dielectric slab introduce a complex input impedance of the transmission line written as:

$$Z_\epsilon = jZ_d \tan\left(\beta_d h\right) \tag{3.7}$$

Where β and Z_d are complex and expressed as:

$$\beta_d = \kappa_o\sqrt{\varepsilon' - j\varepsilon''}, \qquad Z_d = \frac{Z_o}{\sqrt{\varepsilon' - j\varepsilon''}} \tag{3.8}$$

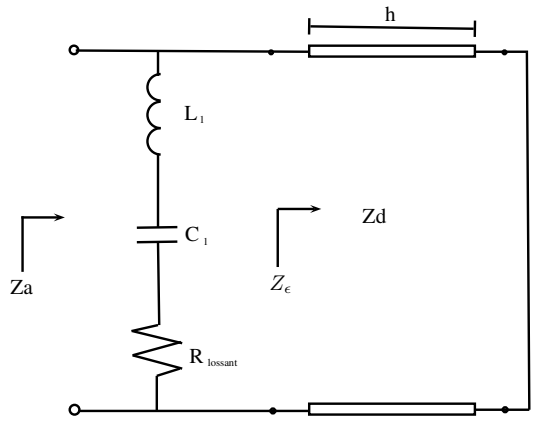

Fig. 3.5: Equivalent Circuit for a Printed Reflect array Antenna

Where κ_o and Z_o are the wave number and impedance of the free space and $(\varepsilon' - j\varepsilon'')$ is complex permittivity of the dielectric sample. The real and imaginary parts after some reductions are then given by:

$$R_\epsilon = Re\left[Z_\epsilon\right] = \frac{Z_o}{a_\epsilon\left({b_\epsilon}^2 + 1\right)} \frac{\sinh\left(2a_\epsilon b_\epsilon h\kappa_o\right) - b_\epsilon \sin\left[2\left(a_\epsilon h\kappa_o\right)\right]}{\cosh\left(2a_\epsilon b_\epsilon h\kappa_o\right) + \cos\left[2\left(a_\epsilon h\kappa_o\right)\right]} \tag{3.9}$$

$$X_\epsilon = Im\left[Z_\epsilon\right] = \frac{Z_o}{a_\epsilon\left({b_\epsilon}^2 + 1\right)} \frac{b_\epsilon \sinh\left(2a_\epsilon b_\epsilon h\kappa_o\right) + \sin\left[2\left(a_\epsilon h\kappa_o\right)\right]}{\cosh\left(2a_\epsilon b_\epsilon h\kappa_o\right) + \cos\left[2\left(a_\epsilon h\kappa_o\right)\right]} \tag{3.10}$$

Where $a = \sqrt{\varepsilon'}$ and $b = \frac{1}{2}\tan\delta$

The reflectarray antenna is not a hundred percent directive antenna and produce dispersion on the reflection wave in the air that depends of the distance between the antenna and the receiver and the frequency. This dispersion can be modelled with a resistor $R_{Lossant}$ in series with the resonance circuit L_1 C_1 as showed in Fig. **??**. This resistor introduce losses in the system and represents the quantity of radiation power that is dispersed in the free space. The impedance than model the dispersion and the resonance circuit is expressed by Z_l in real and imaginary part as:

$$R_l = R_{lossant} \tag{3.11}$$

$$X_l = \frac{\omega^2 L_1 C_1 - 1}{\omega C_1} \tag{3.12}$$

The input impedance Z_a has real and imaginary part. The real part represent losses in the Reflectarray antenna. Z_a is expressed in real and imaginary part as:

$$R_a = \frac{R_\epsilon \mathbf{R}_l^2 + \left(R_\epsilon^2 + X_\epsilon^2\right) \mathbf{R}_l + R_\epsilon X_l^2}{\left(R_\epsilon + R_l\right)^2 + \left(X_\epsilon + X_l\right)^2} \tag{3.13}$$

$$X_a = \frac{X_\epsilon \mathbf{X}_l^2 + \left(R_\epsilon^2 + X_\epsilon^2\right) \mathbf{X}_l + R_l^2 X_\epsilon}{\left(R_\epsilon + R_l\right)^2 + \left(X_\epsilon + X_l\right)^2} \tag{3.14}$$

All the variables are known, expect $R_{lossant}$, that must be solve by numerical methods. In the next section there is explained the way to recover this value by experimental way.

3.3 Open Resonator Technique to characterize the Reflectarray Antenna

The reflecting response of microstrip reflectarray surface can be characterized by inserting a periodic array of identical radiators in the center of the open cavity, as illustrated in Fig. 3.6(a), where R_o gives the radius of the spherical mirror, W is the radius of the Gaussian beam and l is the distance over which the microstrip array grid is fixed. This technique was described and implemented in chapter 2 for dielectric characterization. As a consequence of this, the equivalent circuit of Fig. 2.1 results to be modified as in Fig.3.6(b), with the addition of the impedance Z_a taking into account the presence of the reflecting surface.

It must be observed that, due to the presence of the metallic plane at the center of the cavity, only odd modes are admissible. Each mode has a resonance frequency that is expressed by the equivalent circuit with the elements L_o and C in Fig. 3.6(b), but, by the insertion of the grounded reflecting surface another resonance circuit appears expressed by L_1 and C_1 in Fig. 3.2. Then, two frequencies $f_{1,2}$ are generated for the system for each mode.

The resonant frequencies $f_{1,2}$ are directly obtained from the return loss measurement at the feeding waveguide input of the open resonator. This is loaded with a reflecting surface made of identical square patches having size L and spaced of a distance D. In order to best simulate the infinite array situation, a sufficient large array grid, typically greater than $7X7$, must be considered.

From the circuit reported in 3.6(b), it is straightforward to the deduce the waveguide input impedance Z_i and the reflection coefficient ρ, respectively, given as:

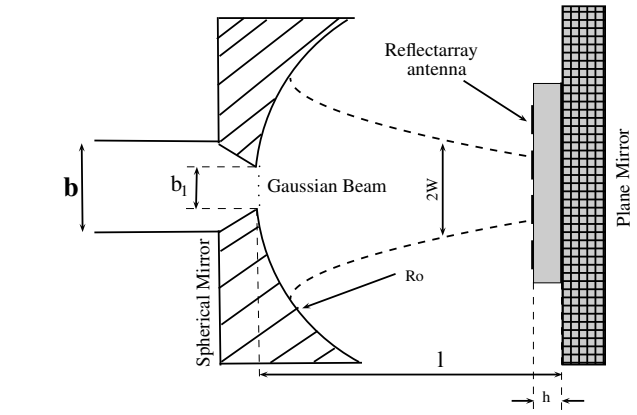

(a) Geometry

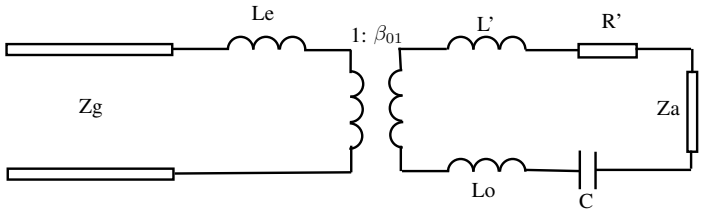

(b) Equivalent Circuit

Fig. 3.6: Open Resonator including a Printed Reflectarray Antenna (a) Geometry (b) Equivalent Circuit

$$Z_i = j\omega L_e + \frac{Z_R}{\beta_{01}^2} \tag{3.15}$$

$$\Gamma = \frac{Z_i - Z_{10}}{Z_i + Z_{10}} \tag{3.16}$$

where

$$Z_R = j\omega L_T + R' + \frac{1}{j\omega C} + Z_a, \tag{3.17}$$

with

$$L_T = L_o + L'$$

$$Z_a = R_a + jX_a$$

The resonant frequencies $f_{1,2}$ appear when the input impedance Z_i in the equation 3.15 turns to zero. Then the impedance Z_a of the reflecting surface can be retrieved once the resonant frequencies are measured in the open resonator system for each mode.

3.3.1 Reflectarray Antenna Reflection characterization considering no losses

The analysis of a reflecting microstrip surface, considering no losses, was treated in section 3.2.1. A equivalent circuit was analysed, but, in this section, the value of the inductance L_u showed in Fig. 3.4 must be adjusted taking into account the Gaussian nature of the beam inside of the cavity [27, 28]. The impedance Z_ϵ from equation 3.4 changes to:

$$Z_\epsilon = jZ_d\left(\beta_d h - \Phi_G\right) \tag{3.18}$$

where Φ_G is the phase shift produced by the Gaussian beam and is given as:

$$\Phi_G = arctan\frac{h}{Z_R} \tag{3.19}$$

The term $Z_R = \sqrt{Rl - l^2}$ into 3.19 represents the Rayleigh distance.

When inserting the equivalent circuit of Fig. 3.4 into that of Fig. 3.2, the resonator will show two resonant frequencies $f_{\{1,2\}}$, relevant of the circuit of Fig. 3.7, which are given as

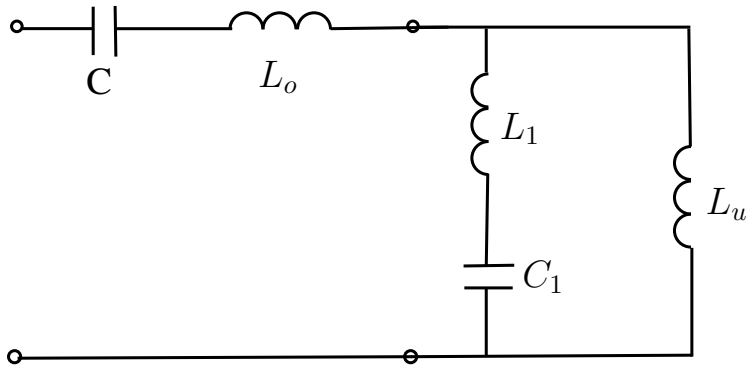

Fig. 3.7: Resonance Equivalent Circuit

$$f_{\{1,2\}} = \frac{1}{2\pi}\sqrt{\frac{b \pm \sqrt{(b^2 - 4a}}{2a}} \tag{3.20}$$

Where

$$a = L_o C(L_1 + L_u)C_1 + C(L_1 L_u)C_1$$

$$b = L_o C + (L_1 + L_u)C_1 + L_u C \tag{3.21}$$

From expresions 3.21, the unknown circuit parameters L_1, C_1 can be easily derived as:

$$L_1 = \frac{C_1 A_1 + B_1}{C_1 E_1} \tag{3.22}$$

$$C_1 = \frac{B_2 E_1 - B_1 E_2}{A_1 E_2 - A_2 E_1} \tag{3.23}$$

Where

$$A_n = (2\pi f_n)^2 L_u - (2\pi f_n)^4 L_u L_o C$$
$$B_n = (2\pi f_n)^2 (L_u + L_o)C - 1$$
$$E_n = (2\pi f_n)^4 (L_u + L_o)C - (2\pi f_n)^2$$

With n=1,2

3.3.2 Reflectarray Antenna Reflection characterization considering losses

The characterization of the reflectarray element response in both amplitude and phase can be done by the open resonator technique considering the losses in the reflecting surface.In section 3.2.2 two types of losses where included, the losses in the dielectric substrate that can be found using the open resonator technique proposed in the previous chapter and the dispersion losses that are explained in this section. The equivalent circuit of the open resonator with the reflectarray antenna considering the losses is showed in Fig. 3.8.

The analysis of the equivalent circuit is done when the resonance frequencies appear, and it happens when the imaginary part of the circuit is zero. Then, the value of the input impedance (Z_i) of the circuit is purely real and deduce the reflection coefficient (Γ) with a real value. Combining Equations 3.15 and 3.16 an expression for Z_R is retrieved as:

$$Z_R = \frac{(1+\Gamma)\,\beta_{01}^2 Z_g}{(1-\Gamma)} - j\omega L_e \beta_{01}^2 \tag{3.24}$$

Inserting 3.24 into 3.17, we obtain two new equations that let to find the values of R_a and Z_a as:

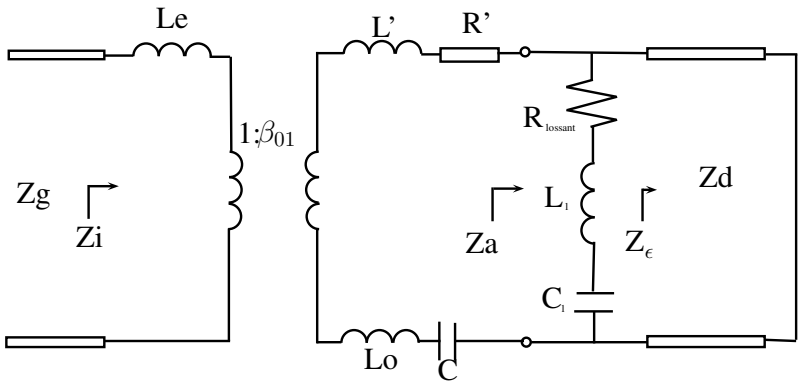

Fig. 3.8: Equivalent Circuit for a Printed Reflect array Antenna

$$R_a = \frac{(1+\Gamma)\,\beta_{01}^2 Z_g}{(1-\Gamma)} - R^{'} \tag{3.25}$$

$$X_a = \frac{1}{\omega C} - \omega\left(L_e\beta_{01}^2 + L_T\right) \tag{3.26}$$

Once the value of R_a and X_a are known, is necessary to solve the equation 3.13 and 3.14 to find the values of the unknown parameters R_l, L_1 and C_1. As we explained in the previous sections, the resonance circuit L_1, C_1 generate two resonance frequencies in the open resonator system. Then is necessary to solve the equation 3.14 for these two resonance frequencies. Considering the fact that R_l has a very low value, it can be depreciated in the resolution of equation 3.14 that changes to a simple second grade equation expressed as:

$$(X_a - X_\epsilon)\,X_l^2 + \left(2X_aX_\epsilon - |Z_\epsilon|^2\right)X_l + |Z_\epsilon|^2 X_a = 0 \tag{3.27}$$

Then, the value of L_1 and C_1 can be easily retrieved as

$$L_1 = \frac{1}{2\pi}\frac{f_1 X_{l1} - f_2 X_{l2}}{{f_1}^2 - {f_2}^2} \tag{3.28}$$

$$C_1 = \frac{1}{2\pi f_1\left(2\pi f_1 L_1 - X_{l1}\right)} \tag{3.29}$$

where $X_{l1,l2}$ are the values of X_l retrieved in equation 3.28 for each resonace$f_{1,2}$ measured in the open resonator.

The value of R_l for each resonance frequency is found solving the equation 3.29, and can be rewritten as:

$$\left(R_a - R_\epsilon\right) R_l^2 + \left(2R_a R_\epsilon - |Z_\epsilon|^2\right) X_l + \left(|Z_\epsilon|^2 + X_l^2\right) R_a - R_\epsilon X_l^2 = 0 \quad (3.30)$$

To solve all the equation is necessary to consider a small change in the input impedance Z_ϵ of the transmission line, that considers a complex permittivity and a Gaussian beam and change from equations 3.9 and 3.10 to:

$$Re\left[Z_\epsilon\right] = \frac{Z_o}{a_\epsilon\left({b_\epsilon}^2 + 1\right)} \frac{\sinh\left(2a_\epsilon b_\epsilon h\kappa_o\right) - b_\epsilon \sin\left[2\left(a_\epsilon h\kappa_o - \phi_G\right)\right]}{\cosh\left(2a_\epsilon b_\epsilon h\kappa_o\right) + \cos\left[2\left(a_\epsilon h\kappa_o - \phi_G\right)\right]} \quad (3.31)$$

$$Im\left[Z_\epsilon\right] = \frac{Z_o}{a_\epsilon\left({b_\epsilon}^2 + 1\right)} \frac{b_\epsilon \sinh\left(2a_\epsilon b_\epsilon h\kappa_o\right) + \sin\left[2\left(a_\epsilon h\kappa_o - \phi_G\right)\right]}{\cosh\left(2a_\epsilon b_\epsilon h\kappa_o\right) + \cos\left[2\left(a_\epsilon h\kappa_o \phi_G\right)\right]} \quad (3.32)$$

3.3.3 Experimental Validations

In order to experimentally validate the reflectarray elements characterization method outlined in the previous section, a K-band open resonator system of Fig. () is adopted. Reflectarray grids of 16 x 16 identical square patches with a spacing $D = 0.65\lambda_o$ are considered for three different patch lengths L (3.2 mm, 3.5 mm and 3.7 mm) as test surfaces. A dielectric substrate of thickness $h = 0.762mm$ and relative permitivity $\epsilon_r = 2.33$ is considered as support. A photograph showing the open resonator system loaded with the test reflecting surface is reported in Fig. () with a particular illustrating grid in Fig. 3.9.

The open resonator system used is designed with a mirror radius $R_o = 529mm$ and the distance $l = 421mm$ between the spherical and the flat mirrors. The resonator is tuned to work at a design frequency $fo = 24GHz$ (The center operating frequency of the reflectarray to be tested), which corresponds to the excitation of $TEM_{0,0,131}$ mode inside the cavity.

The optimization of the waveguide-to-cavity transition is performed by following the approach outlined in [], thus reducing the standard WR62 waveguide height $b = 4.33mm$ to a value of $b_1 = 0.7mm$.

The test setup is mounted into the Microwave Laboratory at University of Calabria, equipped with the complete facilities for both near-field and far-field measurements.

To derive the reflectarray element behaviour, the return loss magnitude at the waveguide input is measured for the three different values of the patch

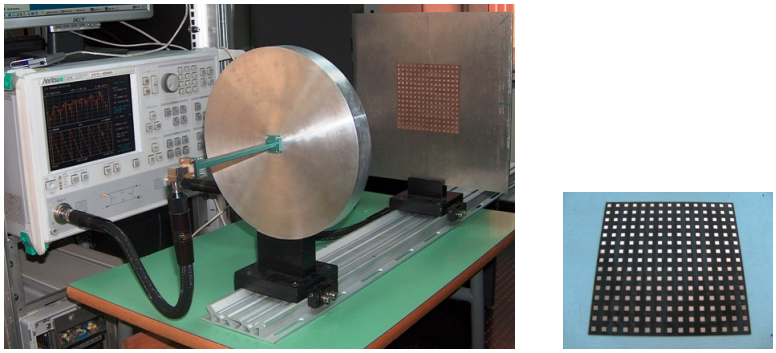

(a) Side View (b) Frontal View

Fig. 3.9: Photograph of (a) Open Resonator System, (b) Realized Reflecting Surface

side L. For all cases, as illustrated in Fig. (3.10-3.12) several resonances couples are visible, corresponding to the various modes excited into the cavity. However, the only couple to be considered is that the equivalent circuit of Fig. 3.6(b) modelled, corresponding to the $TEM_{0,0,131}$ mode, which is associated to an empty cavity resonance $f_o = 24GHz$.

In the presence of each reflecting surface, two resonant frequencies $f_{1,2}$ are produced, as highlighted in the previous section. They can be easily identified in the return loss measurements (Figs. 3.10 -3.12) as follows:

- For a patchside dimension L less than that providing the resonance condition, frequency f_1 is chosen as the nearest one (at the left side) to the resonance frequency f_o of the empty cavity, while the frequency f_2 corresponds to the resonance of the reflectarray grid, easily computed on the basis of the patch dimension L. This is the case corresponding to Fig. 3.10.

- For a patch side dimension L equal to that providing the resonance condition, frequencies $f_{1,2}$ are chosen as those which are equally far form the resonace frequency f_o of the empty cavity. This is the case corresponding to Fig. 3.11.

- For a patch side dimensions L greater than that providing the resonance condition, frequency f_1 is chosen as the nearest one(at the right side) to the resonance frequency f_o of the empty cavity, while the frequency f_2 corresponds to the resonance of the reflectarray grid, again computed on the basis of the patch dimension L. This is the case corresponding to Fig. 3.12.

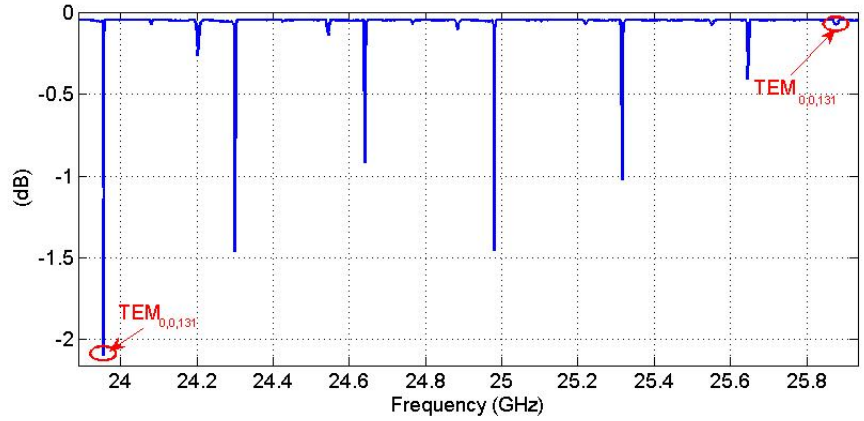

Fig. 3.10: Measured return loss for the case L=3.2mm

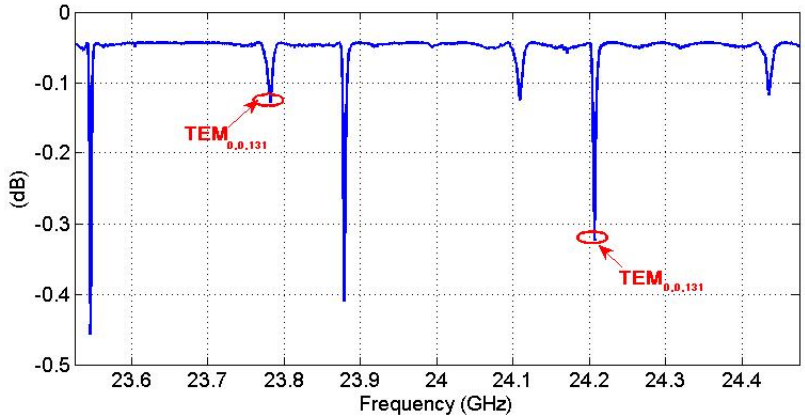

Fig. 3.11: Measured return loss for the case L=3.5mm

The relevant resonances are highlighted in Fig.3.10-3.12 and summarized in Table 3.2.

The measured resonance frequencies $f_{1,2}$ are used to retrieved the values of parameters L_1 and C_1 (See Table 3.2), which are applied into the equivalent circuit of Figure 3.4 to compute the impedance Z_a, subsequently adopted in the circuit of Figure 3.6(b) to obtain the phase of the reflection coefficient relative to the reflectarray grid. Results are reported in Figures as a function of frequency for the three different dimensions of the patch side L. When performing the synthesis of microstrip reflectarray, the reflection phase behavior of the single radiating element is of primary importance, as providing

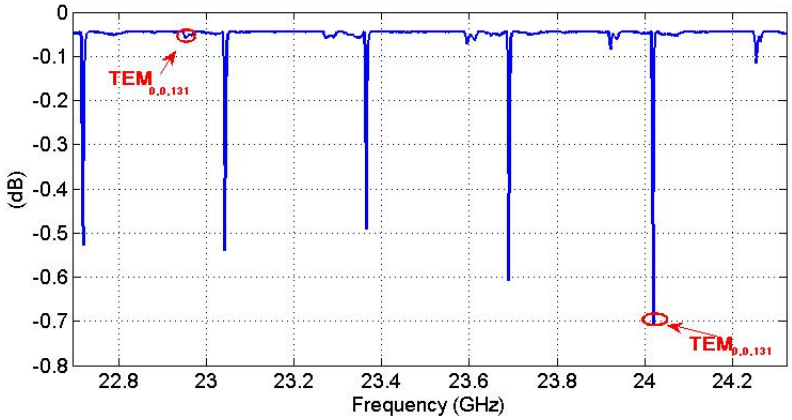

Fig. 3.12: Measured return loss for the case L=3.7mm

Table 3.1: Resonant frequencies $f_{1,2}$ and relatives value of the parameters L_1 C_1.

Patch Length L (mm)	f_1 (Ghz)	f_2 (Ghz)	L_1 (nH)	C_1 (fF)
3.2	23.95	25.88	4.06	7.55
3.5	23.78	24.22	4.24	8.44
3.7	22.95	24.02	4.54	8.70

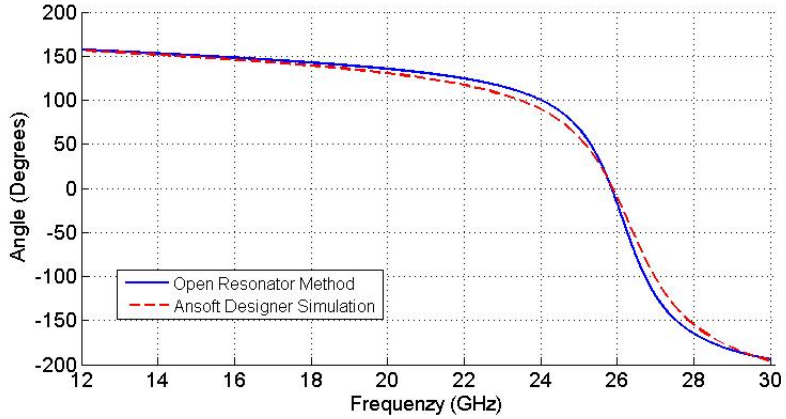

Fig. 3.13: Reflection Phase versus frequency for the case L=3.2mm

the proper dimensions of the tuning parameter (e.g., the patch side L) which are able to guarantee the phase distribution on the array grid assuming the prescribed-field pattern. To validate the results provided by the proposed approach, the reflection phase computed by Ansoft Designer Software (infinite array approach) is also reported in Figures 3.13 - 3.15, and a successful agreement can be observed.

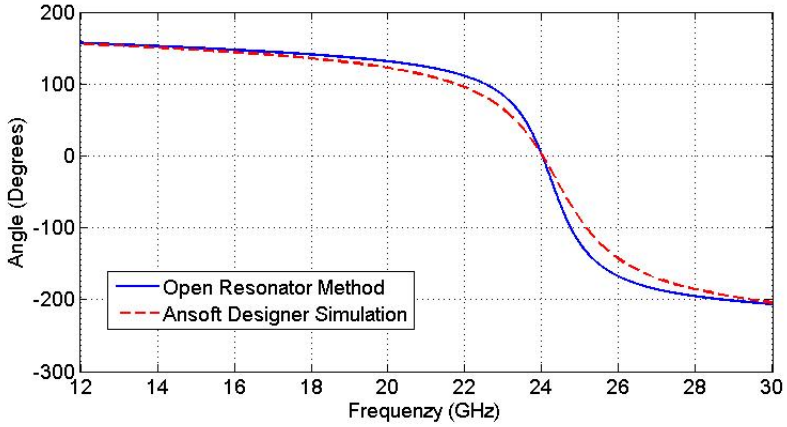

Fig. 3.14: Reflection Phase versus frequency for the case L=3.5mm

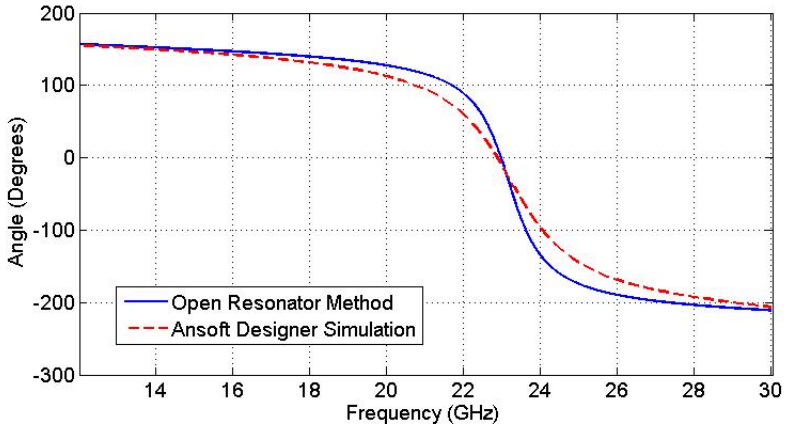

Fig. 3.15: Reflection Phase versus frequency for the case L=3.7mm

Finally, the information retrieved from the three different measurement are combined to obtain the reflection phase design curve versus the patch length L. Again, the effectiveness of the approach is successfully demonstrated in Figure 3.16 by comparison with the results coming from Ansoft Designer Simulations.

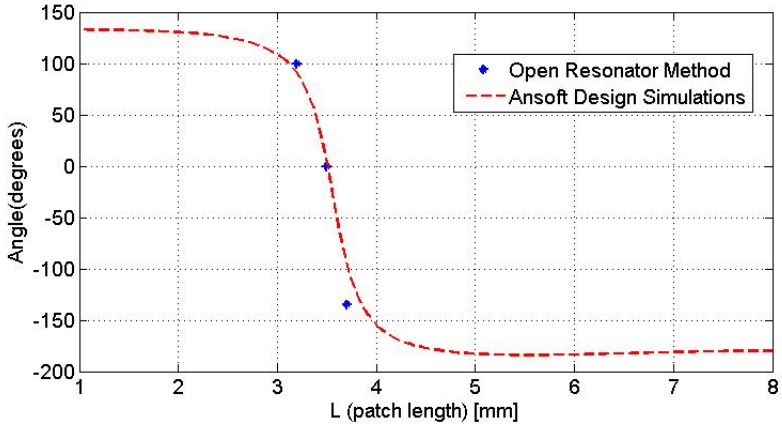

Fig. 3.16: Reflection Phase versus patch length L

The measured resonance frequencies $f_{1,2}$ for each mode are used to retrieved the value of R_l from equation 3.15. Results for the case of $L = 3.5mm$ is reported in Fig. 3.17. To validate the result provided by our proposed approach, the reflection module computed by Ansoft Designer Software (infinite array approach) is also reported and a successful agreement can be observed

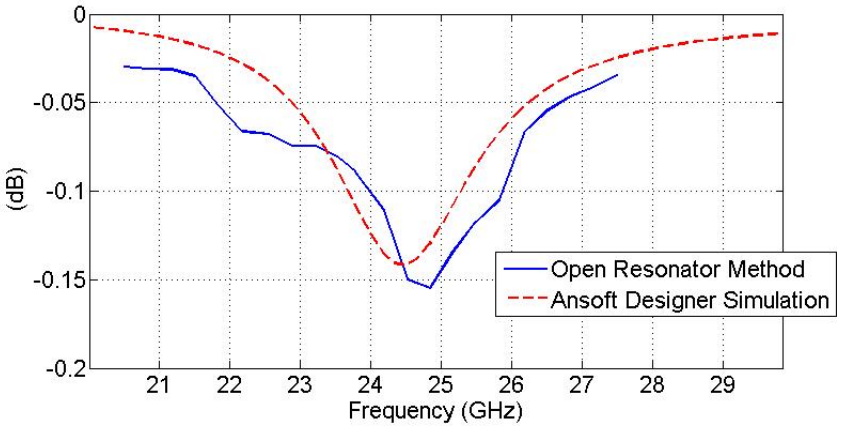

Fig. 3.17: Reflection Module versus frequency for the case of L=3.5mm

Part II

Fabry Perot Antenna Design

4

Fabry Perot Anenna

4.1 Introduction

Sensors, radar, focused power and personal communications highlight growing applications at millimeter wave frequencies, that implies a large amount of transmitting data. However, the adoption of millimeter waves gives some drawback in the antenna design, which cannot be afforded by conventional procedures. In fact, many original solutions like printed antennas on membrane structures [24], reflectarray [54], [55] and many kind of lens antennas have been proposed. Fabry-Perot antennas are a very interesting solution, as providing a high agility in the design-synthesis.

The use of Open Resonators with spherical mirrors as microwave Gaussian Beam Antennas [65], [15] provides a very interesting solution as they can provide very low sidelobes level. They are based on the result that the field map at the mid section of an open resonator shows a gaussian distribution that can be used to illuminate a metallic grid or a dielectric sheet.

Planar Fabry-Perot [1] antennas [15] give a promising solution, as they can provide a high agility in the design-synthesis. The use of a Fabry-Perot interferometric as radiating antenna has been reported in several papers. In [64] the interferometric nature of the double grid operated in long wavelength radiation are discussed using a multiple scattering approach to determine the optimal design parameters. The paper does not report the use of the interferometer as an antenna, but this use is implicitly suggested by the type of structure. The use of metallic planar Fabry-Perot directive antenna, excited by a patch, is proposed in [67]. The structure is simulated by a code based on the method of moment. Other example of at Fabry-Perot antennas are given in [68] and [69]. All these papers demonstrate that this type of antenna has a little operating frequency bandwidth.

In this chapter, a Fabry-Perot antenna, based on an open resonator with rectangular plane mirrors, is presented. A modal solution is used to represent

the electromagnetic field in the cavity. The field is used to compute the coupling with the transition to the feeding waveguide and to the radiating grid.

4.2 The Metallic Fabry Perot Antenna

The antenna is a parallelepiped-al flat structure with a square at metallic base that is coupled by a slot to a rectangular waveguide and a radiating face composed by a metallic sheet were the radiating slots are cut (Fig. 4.1).

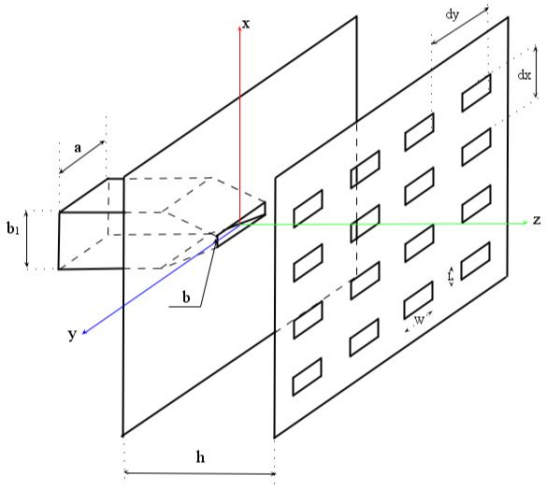

Fig. 4.1: Metallic Fabry-Perot Antenna

The theory analysed in Chapter 1 is used for the cavity feeding by the rectangular waveguide, where a LC electrical circuit represents the resonance frequency in the cavity, but is necessary to add one more analysis to couple the cavity to free space.

4.2.1 Coupling cavity to free space

In the Bethe's original theory [70], the incident field is considered in the absence of the aperture.The magnetic dipole moment is related to incident field as follows:

$$\mathbf{M} = -\alpha_m \mathbf{H}_t \tag{4.1}$$

where H_t is the tangential magnetic field at the center of the aperture and the magnetic polarizability, for small rectangular aperture, is given by ([17]):

$$\alpha_m = \frac{0.132}{lg\left(1+\frac{0.66W}{L}\right)}W^3 \tag{4.2}$$

where W and L are the dimensions of aperture with $L \ll W$.

The radiated field are calculated as the product of the field of a single element, considered as a simple magnetic dipole, and the array factor:

$$E_t = E_{singleelement} \times AF\left(\theta,\phi\right) \tag{4.3}$$

with $E_{singleelement}$ as the field of a single rectangular aperture in the origin with length W and $AF\left(\theta,\phi\right)$ is the array factor, that consider uniform spacing but different amplitude. The array factor is expressed as:

$$AF\left(\theta,\phi\right) = \sum_{g=1}^{M}\sum_{h=1}^{N} I_m(g,h)e^{jk\widehat{r}\cdot\overrightarrow{r_{gh}}} \tag{4.4}$$

where $I_m(g,h)$ is the amplitude for each point-source (g,h) that is equal to the magnetic dipole moment $\mathbf{M}$ evaluated in the point $(x,y) = \left(g-\frac{M-1}{2}\right)dx$, $\left(h-\frac{N-1}{2}\right)dy$, while $\widehat{r} = \widehat{x}\sin\theta\cos\phi + \widehat{y}\sin\theta\sin\phi + \widehat{z}\cos\theta$ and $\overrightarrow{r_{gh}} = \left(g-\frac{M-1}{2}\right)dx\widehat{x} + \left(h-\frac{N-1}{2}\right)dy\widehat{y}$ with M and N as the number of elements in $\widehat{x}$ and $\widehat{y}$

To find the field of single element is necessary to determine the potential function $\mathbf{F}$ for a magnetic dipole where $W < \lambda$:

$$F\left(x,y,z\right) = \frac{\varepsilon}{4\pi}\int_C I_m\left(x^{'},y^{'},z^{'}\right)\frac{e^{(-jkR)}}{R}dl^{'} \tag{4.5}$$

where (x,y,z) represent the observation point coordinates, $\left(x^{'},y^{'},z^{'}\right)$ represent the coordinates of the source, R is the distance from any point on the source to the observation point, and path C is along the length of the source.

I_m is the current distribution for a thin dipole and can be written as:

$$I_m\left(x^{'}=0,y^{'},z^{'}=0\right) = \begin{cases} \widehat{y}\sin\left[k\left(\frac{W}{2}-y^{'}\right)\right], & 0 < y^{'} < W/2 \\ \widehat{y}\sin\left[k\left(\frac{W}{2}+y^{'}\right)\right], & -W/2 < y^{'} < 0 \end{cases} \tag{4.6}$$

The transformation between rectangular and spherical components is given, in matrix form:

$$\begin{bmatrix} F_r \\ F_\theta \\ F_\phi \end{bmatrix} = \begin{bmatrix} \sin\theta\cos\phi & \sin\theta\sin\phi & \cos\theta \\ \cos\theta\cos\phi & \cos\theta\sin\phi & -\sin\theta \\ -\sin\phi & \cos\phi & 0 \end{bmatrix} \begin{bmatrix} F_x \\ F_y \\ F_z \end{bmatrix} \tag{4.7}$$

Because the potential function $\mathbf{F}$ exists only in $\widehat{y}$ direction implies that $E_r = 0$ and E_θ and E_ϕ are expressed as:

$$E_\theta = -j\frac{e^{-jkR}}{2\pi R}\left[1+\frac{1}{jkr}\right]\frac{\cos\phi}{1-\sin^2\theta\sin^2\phi}\left[\cos\left(\frac{kW}{2}\sin\theta sin\phi\right)-\cos\left(\frac{kW}{2}\right)\right] \tag{4.8}$$

$$E_\phi = -j\frac{ke^{-jkR}}{2\pi R}\left[1+\frac{1}{jkr}\right]\frac{\cos\theta\sin\phi}{1-\sin^2\theta\sin^2\phi}\left[\cos\left(\frac{kW}{2}\sin\theta sin\phi\right)-\cos\left(\frac{kW}{2}\right)\right] \tag{4.9}$$

4.2.2 Modeling and Results

Following the reasoning of previous paragraphs, the antenna depicted under (Fig. 4.1) is considered. Two array are considered: An array of 8x8 elements,with dimensions h=9.8mm; dx=dy=12.5mm; W=6.35mm; L=2mm and an array of 16x16 elements, with dimensions h = 9.8mm; dx = 13mm; dy = 13mm;W = 6.35mm; L = 2mm.

The analysis of coupling between a rectangular cavity feeding waveguide and the planar open cavity is performed by taking into account the theory explained in chapter 1. The result is reported in Fig. 4.2 and the best coupling is when the waveguide height has a value around 1.7 mm. Then, the feeding was done with a transition in the waveguide from an aperture with dimensions a = 15.8; b = 7.8mm, into an aperture of a = 15.8; b = 1.7mm.

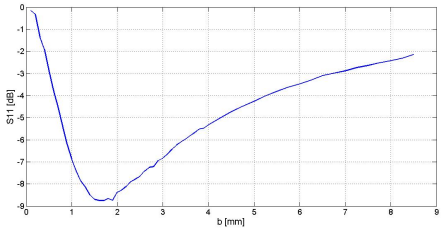

Fig. 4.2: Return loss vs. waveguide height

A first preliminary result of the radiation diagram at 15 GHz using the simplified analysis of the proposed antenna and HFSS simulation are reported in Fig. 4.3 and 4.4.

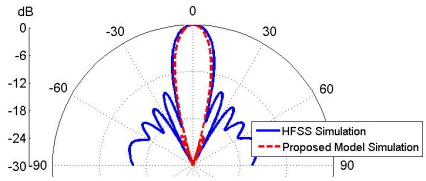

Fig. 4.3: Radiated Field E_ϕ, with $\phi = 90$, at 15 GHz considering an array 8x8 elements

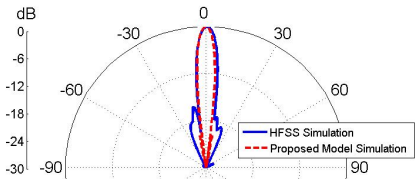

Fig. 4.4: Radiated Field E_ϕ, with $\phi = 90$, at 15 GHz considering an array of 16x16 elements

4.3 The improved Bandwidth Fabry-Perot Antenna

In this section we consider a dielectric partially filled rectangular Fabry-Perot antenna as depicted under Fig. 4.5.

4.3.1 Field in the partially filled cavity

The solution for the field computed in an empty cavity, are still valid for $-l \leq z \leq h1 - l$. When we consider a partially filled cavity, the quasi transverse electromagnetic field in the dielectric, for $h1 - l \leq z \leq h1 + h2 - l$, is:

$$H_{2y} = -jA_\epsilon \frac{k}{Z_w} \frac{\pi}{l} e^{-j\pi p} cos\left(\frac{\pi\xi}{M_a + \gamma}\right) cos\left(\frac{\pi\eta}{M_b + \gamma}\right) sin(\frac{\pi z}{2l_2}) \qquad (4.10)$$

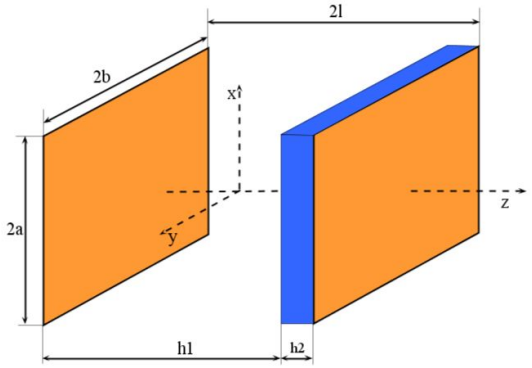

Fig. 4.5: Rectangular Open resonator partiallly filled with dielectric substrate

and the x component of electric field

$$E_{2x} = B_\epsilon \left[\varepsilon k^2 - \frac{\sqrt{\varepsilon} k}{2l} \frac{\pi^2}{(M_a + \gamma)^2} \right]^2 2e^{-j\pi p} cos\left(\frac{\pi \xi}{M_a + \gamma} \right) cos\left(\frac{\pi \eta}{M_b + \gamma} \right) cos(\frac{\pi z}{2l_2}) \tag{4.11}$$

$$E_{2x} = Z_{s2} H_{2y} \tag{4.12}$$

where $l2 = h1 + h2 - l$. For $z = h1 - l$ the field in the empty part, (25,26), and the field in dielectric filled part must be equal, so we can find A and B.From the continuity of tangential fields on interface air dielectric

$$A_\epsilon = \frac{1}{\varepsilon} \frac{\sin\left[\frac{\pi}{2l}(h1 - l)\right]}{\sin\left[\frac{\pi}{2l_2}(h1 - l)\right]} \tag{4.13}$$

$$B_\epsilon = \frac{Z_{s2}}{Z_s} A_\epsilon \tag{4.14}$$

4.3.2 Modelling and Results

In the following results the radiation fields are reported for an antenna where a dielectric sheet of dielectric load the cavity. With reference to Fig. 4.6 an array of 8x8 elements and the dimensions considered are: h1 = 8:637mm; h2 = 0:762; ” = 2:33;W = 6:35mm; L = 2mm; dx = 12:5mm; dy = 12:5mm; b = 1:7mm

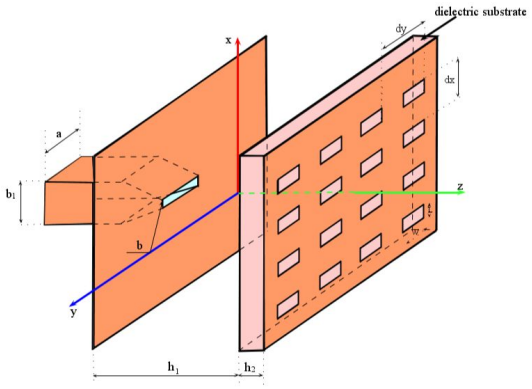

Fig. 4.6: Partially filled cavity circuit

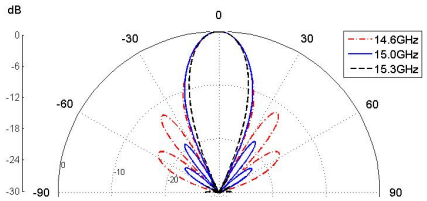

Fig. 4.7: Radiated Field E_ϕ (Array of 8x8 elements)

In Fig. 4.7 the radiation diagram for several frequencies is reported.

From previous results arise that the introduction of a dielectric sheet in the cavity improve the frequency working bandwidth of the antenna.

4.4 Experimental Validations

In order to experimentally validate the method outlines in the previous section, with reference to Fig. 4.10, an array antenna of 8x8 elements for a K-band frequency is designed where the dimensions considered are: h1 = 8.637mm; h2 = 0.762mm; $\varepsilon = 2.33$; W = 6.35mm; L = 2mm; dx = 12:5mm; dy = 12:5mm; b = 1:7mm.

The optimization of the waveguide-to-cavity transition is performed by following the approach outlined in [26], thus reducing the standard WR62 waveguide height $b = 4.33mm$ to a value of $b = 2mm$. The antenna implemented is showed in Figure 4.8.

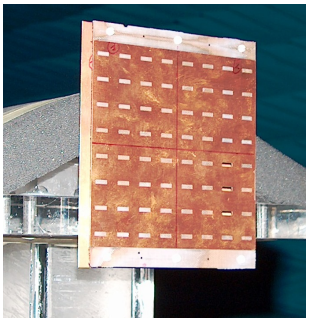

Fig. 4.8: Photograph of the antenna

The test setup is mounted into the Microwave Laboratory at University of Calabria, equipped with complete facilities for both nearfield and far-field measurements.The dimensions of the anechoic chamber are 8.0 m (long), 6.0 m (wide) and 4.0 m (high).

The far-field measurement was done under the scheme showed in Fig.4.9,.The radiation patterns has been measured at a distance of 1.20 [m], largest than the minimum distance required to considered far field radiation $2D^2/\lambda = 0.99[m]$, where D is the largest physical linear dimension of the antenna, that is 100 [mm] and λ is equal to 20.20 [mm] at 14.85 [GHz].

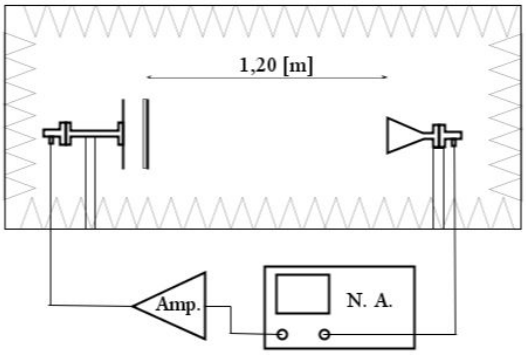

Fig. 4.9: Far-Field Scheme Measurement

In Fig. 4.10, some photographs show the Fabry-Perot antenna mounted in the anechoic chamber for the far field measurement considering vertical and horizontal polarization. The receiver antenna is a horn antenna working in K

band. The transmitter and receiver antenna are aligned to get accurate results.

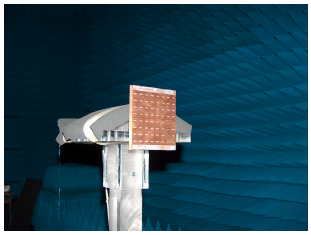

(a) Fabry-Perot Antenna to be tested (Transmitter)

(b) Horn Antenna (Receiver)

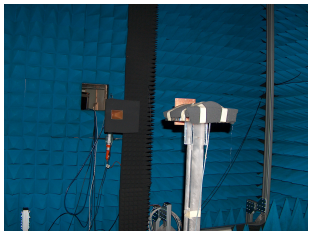

(c) Vertical Polarization Test

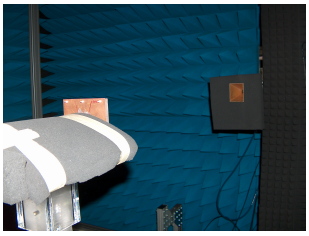

(d) Horizontal Polarization Test

Fig. 4.10: Photograph of the Fabry-Perot Antenna prototype into the anechoic chamber

The comparison of gain versus frequency between empty cavity and the partially filled cavity is reported under Fig. 4.11 where the bandwidth at -3 **dB** of the antenna with an empty cavity is around 0.27 GHz while the measured bandwidth at -3 **dB** of the antenna with a partially filled cavity is around 0.40 GHz. These results give a bandwidth improvement more than 40% when a dielectric sample is inserted in the antenna. The measurement gain result is showed too.

The radiating patterns for E_ϕ at $\theta = 90$ for two different frequencies, 14.6 [GHz] and 14.85 [GHz] are shown in Fig. 4.12. A qualitative agreement is obtained in the behaviour of the antenna, where the measurement results are compared with the proposed approach.

The nearfield measurement was done under the scheme showed in Fig.4.13, considering a planar test setup, where the antenna under test was mounted in a stationary fashion (fixed), 180 [mm] far from the measurement system. A waveguide WR62 is used as a field probe, that performs a flat rectangular

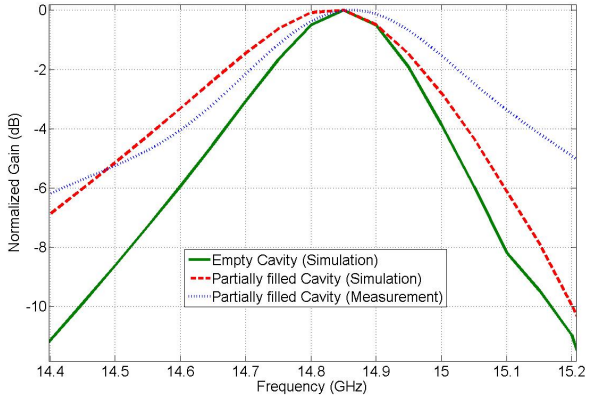

Fig. 4.11: Return loss vs. waveguide height

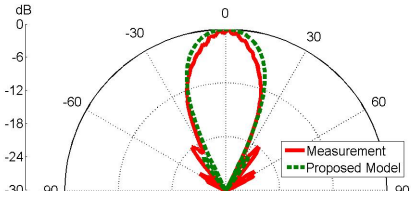

(a) 14.6GHz

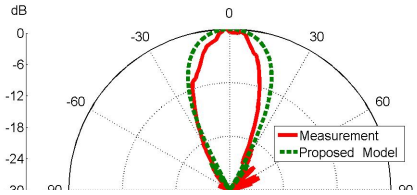

(b) 14.85 GHz

Fig. 4.12: Radiation Field at $\phi = 90$

surface, with measurements in a grid of 63X63 points with a step of 10 [mm] along the planar surface in both horizontal (X) and vertical (Y) directions at 14.85GHz.

In Fig. 4.14, the Fabry-Perot antenna under test in nearfield configuration is presented. The side view shows the waveguide as a field probe and the back view show how all the system is isolated to get the best results in the measurement procedure.

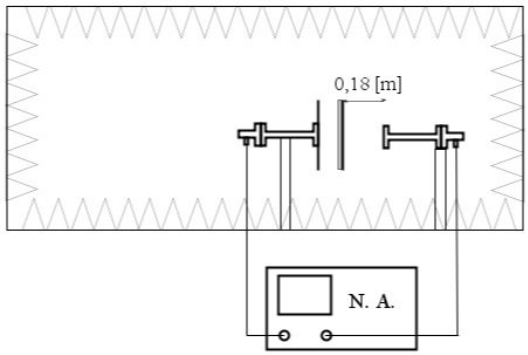

Fig. 4.13: NearField Scheme Measurement

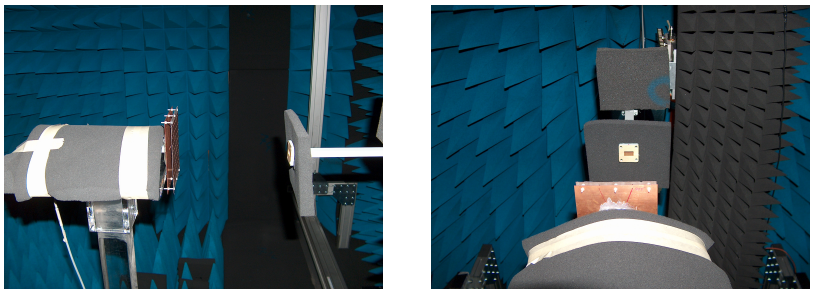

(a) Side View (b) Back View

Fig. 4.14: Photograph of the Near Field Measurement

Fig. 4.15 presents the near field measurement,a grid of 3969 points that as showed in the figure, represents a planar surface from -15λ to -15λ in both X and Y directions, that combined generated the near field result, where is clear the good performance of the antenna.

These result complements the far field measurement and confirm the theory proposed in these chapter. New models can be proposed from these results taking into account that the dielectric sample help to increase the bandwidth.

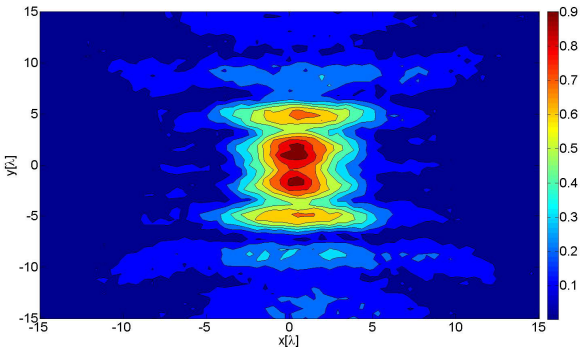

Fig. 4.15: NearField Measurement

Conclusions

1. An improved open resonator technique for the retrieval of dielectric complex permittivity has been proposed in this paper. An explicit equivalent circuit description has been obtained, which provides a simple and accurate prediction of the cavity behaviour, thus avoiding the use of a cumbersome numerical analysis for the design of the structure.

2. By exploiting a simple equivalent circuit, the proposed approach takes properly into account the coupling with the feeding waveguide, as well as the ohmic and the diffraction losses of the cavity. Three different grounded dielectric sheets, usually adopted for microwave planar circuits, have been successfully used for K-band experimental validations of the proposed technique.

3. The use of an open cavity has been proposed in this work to characterize variable patches microstrip reflectarray. An equivalent circuit including both the open resonator and the reflecting surface has been adopted to recover the reflection phase versus the patch length from return loss measurements at the feeding waveguide input. Experimental validations have been successfully discussed on K-band reflectarray prototypes.

4. The proposed characterization method is particularly suitable for millimeter-wave applications, where the reduced dimensions make impractical the adoption of standard techniques.

5. An open planar cavity antenna has been presented in this work, by providing an equivalent simplified circuit and obtaining both input characteristics and radiation diagrams of the antenna. A solution to the problem of bandwidth enlargement has been provided. The experimental characterization of the antenna has been reported.

6. For future developments, the following comments are in order:

- The coupling of an open spherical cavity through a circular hole has been frequently used, but no adequate study exists. It can be dealt by using a modal expansion in terms of Laguerre polynomials for the cavity and considering only one azimuthal mode index, which gives a simple representation of the problem;

- The open resonator method can be applied to any quasiplanar composite scattering object to measure the amplitude and phase of the scattered electromagnetic field. Grounded metallic strips, patches or frequency selective surfaces can be usefully characterized in this way.

- The development of a synthesis procedure using in the Fabry-Perot design by the use of the positions and size of the radiating slots will be considered;
- Several types of radiating elements and feeding structures can be considered;

References

1. C. Fabry and A. Perot (1899), Theorie et Applications d'une Nouvèlle Method de Spectroscopie Interfèrentielle, Ann Chim Phys., Vol. 16: 115–143.
2. R.H. Dick (1958), "Molecular amplifications and generation systems and methods", U.S. Patent 2 851 652.
3. A. M. Prokhorov (1958), "Molecular amplifier and generator for submillimeter waves", JETP (USSR), Vol. 34:1140–1141.
4. A. L. Schawlow and C. H. Townes (1958), "Infrared and optical masers", Phys. Rev., Vol. 29: 1940–1949.
5. G. D. Boyd and J. P. Gordon, (1961), Confocal multimode resonator for millimeter through optical wavelength masers, Bell Sys. Tech. J., Vol. 40: 489-508.
6. G. D. Boyd and H. Kogelnik, (1962), Generalized confocal resonator theory, Bell Sys. Tech. J., Vol. 41: 1347–1369.
7. P. O. Clark, (1964). A self consistent field analysis of Spherical-Mirror Fabry-Perot Resonators, Proc. of the IEEE, Vol. 53, No. 1: 36–41
8. H. Kogelnik, T. Li, (1996), Laser beam and resonator, Proc. IEEE, Vol. 54: 1312-1329.
9. A. L. Cullen and P. K. Yu (1979), "Complex source-point theory of the electromagnetic open resonator", Proc. R. Soc. London, Sr. A 366: 155-171.
10. R. N. Clarke, C. B. Rosemberg, (1982), Fabry-Perot and Open Resonator at Microwave and Millimeter wave frequencies, 2-200 GHz, J. Phys. E: Sci. Instrum., Vol. 15: 9–24
11. A. Perrenoud, M.Q. Tran, B. Isac, (1986), On the design of open resontaro for quasi-optical gyratron, Int. J. of Infrared and Millimeter Waves, Vol. 7: 427-446.
12. G. Di Massa, R. Fedele, G. Miano, C. Nappi (1990), A beat wave experiment in open resonator, Physica Scripta, Vol. T30: 122–126.
13. S. R. Seshadri (1998), "Electromagnetic Gaussian beam", J. Opt. Soc. Am. A 15:2712–2719.
14. G. Di Massa, L. Boccia, G. Amendola, (2005), A Gaussian beam antenna based on an open resonator, The European Conference on Wireless Technology, Paris, France.
15. G. Di Massa, L. Boccia, G. Amendola, (2005), Gaussian beam antennas based on open resonator structures, 28th ESA Antenna Workshop on Space Antenna System and Technologies.

16. R. Sauleau, P. Coquet, D. Thouroude, J. P. Daniel and T. Matsui, (2003), Radiation Characteristics and Performance of Millimeter-Wave Horn-Fed gaussian Bean Antennas, IEEE Trans. Antennas and Propagation, Vol. 51: 379-386.
17. A. L. Cullen, P. R. Yu, (1979), Complex source-point theory of the electromagnetic open resonator, Proc. R. Soc Lonc. A., Vol. 366: 155–171.
18. G. Di Massa, D. Cuomo, A. Cutolo, G. Delle Cave, (1989), Open resonator for microwave application, IEE Proc. H, Vol. 136: 159–164.
19. V. N. Rodionova, A. Ya. Slepyan, G. Ya. Slepian, (1991), Oliner model for quasioptical resonator to rectangular waveguide coupling elements, Electronic Letters, Vol. 27: 1427–1428.
20. O. Bucci, G. Di Massa, (1992), Open resonator powered by rectangular waveguide, IEE Proceedings-H, Vol. 139: 323–329.
21. M. A. Leontovich , (1944), Statistical Physics, OGIZ, Moskow.
22. M.A. Leontovich , Fock V.A., (1948), Investigation of Radio Wave Propagation, ed. B.A. Vendeski, AN SSSR, Moskow, 13–39.
23. K. Kurokawa, (1969), An introduction to theory of microwave circuits, Academic Press, New York.
24. S. Costanzo, I. Venneri, G. Di Massa, and A. Borgia (2010) "Benzocyclobutene as substrate material for planar millimeter wave structures: Dielectric characterization and application", International Journal of Infrared and Millimeter Waves, 31:66–77.
25. U. C. Hasar and I. Y. Ozbek (2011) "Complex permittivity determination of lossy materials at millimeter and terahertz frequencies using freespace amplitude measurements", Journal of Electromagnetic Waves and Applications, 25:2100–2109
26. G. Addamo, G. Virone, D. Vaccaneo, R. Tascone, O. A. Peverini, and R. Orta (2010) "An adaptive cavity setup for accurate measurements of complex dielectric permittivity", Progress In Electromagnetics Research, 105:141–155
27. U. C. Hasar (2010) "Unique permittivity determination of lowloss dielectric materials from transmission measurements at microwave frequencies", Progress In Electromagnetics Research, 107:31–46
28. G.D. Dester, E. J. Rothwell, M. J. Havrilla, and M. W. Hyde IV (2010) "Error analysis of a two layer method for the electromagnetic characterization of conductor backed absorbing material using an openended waveguide probe", Progress In Electromagnetics Research B, 26:1–21
29. R. N. Clarke and C. B. Rosemberg (1982) "Fabryperot and open resonators at microwave and millimeter wave frequencies, 2-200 GHz", J. Phys. E: Sci. Instrum., 15:9–24
30. P. K. Yu and A. L. Cullen (1982) "Measurement of permittivity by means of an open resonator. I Theoretical", Proc. R. Soc. Lond. A, 380:49–71
31. A. C. Linch (1982) "Measurement of permittivity by means of an open resonator. II Experimental", Proc. R. Soc. Lond. A, 380:73–76
32. A. L. Cullen, P. Williams, and A. D. Nagenthiram (1972) "Improvement in open resonator permittivity measurement", Electronic Letters, 8:577-579
33. R. J. Cook, R. G. Jones, and C. B. Rosemberg (1974) "Comparison of cavity and open resonator measurements of permittivity and loss angle at 35 GHz", IEEE Trans. on Instrum. Measurements, 23:438–442
34. R. G. Jones (1976) "Precise dielectric measurements at 35 GHz using an open microwave resonator", Proc. IEEE, 123:285–290

35. R. J. Cook and R. G. Jones (1976) "Correction to open resonator permittivity and loss measurements", Electronic Letters, 12:1–2
36. T. M. Hirvonen, P. Vainikainen, A. Lozowski, and A. V. Raisanen (1996) "Measurement of dielectrics at 100 GHz with an open resonator connected to a network analyzer", IEEE Trans. on Instrum. Measurements, 45:780–786
37. W. F. P. Chan and B. Chambers (1987) "Measurement of non planar dielectric samples using an open resonator", IEEE Trans. on MMT, 35:429–434
38. B. Komiyama, M. Kiyokawa, and T. Matsui (1991) "Open resonator for precision dielectric open resonator for precision dielectric", IEEE Trans. on MMT, 39:1792–1796
39. S. N. Dudorov, D. V. Lioubtchenko, J. A. Mallat, and A. V. Risnen (2005) "Differential open resonator method for permittivity measurements of thin dielectric film on substrate", IEEE Trans. on MMT, 54:1916–1920.
40. Y. F. Gui, W. B. Dou, P. G. Su, and K. Yin (2009) "Improvement of open resonator technique for dielectric measurement at millimetre wavelengths", IET Microw. Antennas Propag., 3:1036–1043.
41. Y. F. Gui, W.B. Dou, and K. Yin (2009) "Open resonator technique of non planar dielectric objects at millimeter wavelengths", Progress In Electromagnetics Research M, 9:185–197.
42. J. Huang, (1995) "Analysis of a microstrip reflectarray antenna for micro spacecraft applications", TDA Progress Report 42-120: 153–173.
43. J. Huang, (1996) Capabilities of printed reflectarray antennas, in Proceedings of the IEEE International Symposium on Phased Array Systems and Technology, pp. 131134.
44. D. Berry, R. Malech, and W. Kennedy, (1963) The reflectarray antenna, IEEE Transactions on Antennas and Propagation, vol. 11, no. 6: 645-651.
45. H. Fang, M. Lou, J. Huang, L.M. Hsia, and G. Kerdanyan, (2002) Design and development of an inflatable reflectarray antenna, IPN Progress Report 42-149:1–18.
46. R. D. Javor, X. D.Wu, and K. Chang, (1995) Design and performance of a microstrip reflectarray antenna, IEEE Transactions on Antennas and Propagation, vol. 43, no. 9: 932-939.
47. J. Huang and A. Encinar, (2007) Reflectarray Antennas, IEEE Press, NY, USA.
48. D. M. Pozar, S. D. Targonski, and H. D. Syrigos, (1997) Design of millimeter wave microstrip reflectarrays, IEEE Transactions on Antennas and Propagation, vol. 45, no. 2: 287296.
49. J. C. Ginn, B. A. Lail, and G. D. Boreman,(2007) Phase characterization of reflectarray elements at infrared, IEEE Transactions on Antennas and Propagation, vol. 55, no. 11 I:2989-2993.
50. D. M. Pozar, S. D. Targonski, and R. Pokuls, (1999) A shaped-beam microstrip patch reflectarray, IEEE Transactions on Antennas and Propagation, vol. 47, no. 7: 11671173.
51. A. Kelkar, (1991) FLAPS: conformal phased reflecting surfaces, in Proceedings of the 1991 IEEE National Radar Conference, pp. 5862, March 1991.
52. J. Huang and R. J. Pogorzelski, (1998) A ka-band microstrip reflectarray with elements having variable rotation angles, IEEE Transactions on Antennas and Propagation, vol. 46, no. 5:650-656.
53. L. Boccia, F. Venneri, and G. Di Massa, (2001) A Varactor Loaded Reflectarray Antenna, in Proceedings of the International Conference on Electromagnetics in Advanced Applications (ICEAA01).

54. F. Venneri, S. Costanzo, G. Di Massa et al., (2012) Beam-scanning reflectarray based on a single varactortuned element, International Journal of Antennas and Propagation, vol. 2012, Article ID 290285, 5 pages.
55. F. Venneri, S. Costanzo, and G. Di Massa, (2012) Reconfigurable aperturecoupled reflectarray element tuned by single varactor diode, Electronics Letters, vol. 48:68-69.
56. F. Venneri, S. Costanzo, G. Di Massa, and G. Angiulli, (2005) An improved synthesis algorithm for reflectarrays design, IEEE Antennas and Wireless Propagation Letters, vol. 4, no. 1:258-261.
57. F. Venneri, S. Costanzo, G. Di Massa, P. Corsonello, and M. Salzano, (2012) Design of a reconfigurable reflectarray based on a varactor tuned element, in Proceedings of the European Conference on Antennas and Propagation (EuCAP12), Prague, Czech Republic.
58. R. C. Hansen, (2009) Phase Array Antennas, Wiley Sons,New York, NY, USA.
59. F. C. E. Tsai and M. E. Bialkowski, (2002) An equivalent waveguide approach to designing of reflect arrays with the use of variablesize microstrip patches, Microwave and Optical Technology Letters, vol. 34, no. 3:172-175.
60. F. C. E. Tsai and M. E. Bialkowski,(2003) Designing a 161-element Ku-band microstrip reflectarray of variable size patches using an equivalent unit cell waveguide approach, IEEE Transactions on Antennas and Propagation, vol. 51, no. 10: 2953 2962.
61. J. C. Ginn, B. A. Lail, and G. D. Boreman, (2007) Phase characterization of reflectarray elements at infrared, IEEE Transactions on Antennas and Propagation, vol. 55, no. 11 I: 29892993.
62. M. Bozzi, S. Germani, and L. Perregrini, (2004) A figure of merit for losses in printed reflectarray elements, IEEE Antennas and Wireless Propagation Letters, vol. 3, no. 1:257-260.
63. F. A. Tahir, (2011) Electromagnetic modeling of microstrip reflectarrays using scale changing technique [Ph.D. thesis], Universit di Toulouse.
64. Adams J. L., (1981) The application of double grids as Fabry-Perot Interferometer, J Optics (Paris), 12, No 2:105–113.
65. Sauleau R., Coquet Ph., Daniel J.P., Matsui T., Hirose N., (1998) Study of Fabry-Perot Cavities with metallic mesh mirrors using equivalent circuit models. Comparision with experimental results in the 60 GHz band, International Journal of Infrared and Millimeter waves, 19, No 12:1693–1710.
66. A.P. Feresidis, J.C. Vardaxoglou, (2001) High gain planar antenna using optimised partially rejective surface, IEE Proc. Microw. Antennas Propag.,148, No 6:345–350.
67. N. Gullerin, S. Enoch, G. Tayeb, P. Sabouroux, P. Vincent, H. Legacy, (2006) A metallic Fabry-Perot Directive Antenna, IEEE Trans. Ant. Propag., 54,No.1:220–224.
68. Hosseini, S.A. and Capolino, F. and De Flaviis, F., (2009) Design of a single feed 60 GHz planar metallic Fabry-Perot cavity antenna with 20 dB gain, IEEE International Workshop on Antenna Technology, iWAT.
69. Voytovich N.I., Ershov A. V., Bukharin V.A., Repin N.N.Flat (2012) Cavity Antenna, 6th European Conference on Antennas and Propagation (EUCAP).
70. H.A Bethe, *Theory of Difraction from Small Holes* The Phisical Review,66, pp 163-182, 1944.

Author Publications

Book Chapter

1. Sandra Costanzo, Giuseppe Di Massa and **H. O. Moreno**, (2012) *Microwave Open Resonator Techniques - Part II: Applications* in **"Microwave Materials Characterization"**, Sandra Costanzo, **INTECH**, Croatia.

International Journals Publications

1. G. Di Massa, S. Costanzo, **H. O. Moreno**, (2012) Accurate Circuit Model of Open Resonator System for Dielectric material Characterization, Journal of Electromagnetic Waves and Applications, Vol. 26:783-794.

2. G. Di Massa, S. Costanzo, **H. O. Moreno**, (2012) "Open Resonator System for Reflectarray Elements Characterization", International Journal of Antennas and Propagation, Vol. 2012, Article ID 912809, 7 pages.

3. S. Costanzo, F. Spadafora, **H. O. Moreno**, F. Scarcella, G. Di Massa, (2013) "Multiband Software Defined Radar for Soil Discontinuities Detection", Journal of Electrical and Computer Engineering, Vol. 2013, Article ID 379832, 6 pages.

4. Sandra Costanzo, Francesco Spadafora, Giuseppe Di Massa, Antonio Borgia, Antonio Costanzo, Gianluca Aloi, Pasquale Pace, Valeria Loscri, and **Hugo O. Moreno**, (2013) Potentialities of USRP-Based Software Defined Radar Systems, Progress in Electromagnetism Research B, Vol. 53: 417-435.

5. Sandra Costanzo, Francesco Spadafora, Antonio Borgia, **Hugo O. Moreno**, Antonio Costanzo, and Giuseppe Di Massa, (2013) "High Resolution Software Defined Radar System for Target Detection", Journal of Electrical and Computer Engineering, Vol. 2013, Article ID 573217, 6 pages.

International Conferences

1. S. Costanzo, G. Di Massa, **H. O. Moreno**, (2012) "Improved Open Resonator Technique for Dielectric Characterization ", 6th European Conference on Antennas and Propagations (EUCAP), Prague, Czech Republic.

2. S. Costanzo, G. Di Massa, **H. O. Moreno**, (2012) "Equivalent Impedance Retrieval of Planar Surfaces by Open Resonator Technique", XIX Riunione Nazionale di Elettromagnetismo (RiNEm), Rome, Italy.

3. G. Di Massa, **H. O. Moreno**,S. Costanzo, (2013) "Simplified Model of a Fabry-Perot Antenna", 7th European Conference on Antennas and Propagations (EUCAP), Gothenburg, Sweden.

4. Sandra Costanzo, Francesco Spadafora, Antonio Borgia, **H. O. Moreno**, Antonio Costanzo and Giuseppe Di Massa, (2013) "High resolution Software Defined Radar System for Target Detection" The 2013 World Conference on Information Systems and Technologies, Algarve, Portugal.